NATIONAL TRANSPORTATION SAFETY BOARD

Office of Research and Engineering
Washington, D.C. 20594

December 10, 2009

Aircraft Performance

Group Chairman's Aircraft Performance Study
by John O'Callaghan

A. ACCIDENT

Location:	Weehawken, NJ
Date:	January 15, 2009
Time:	15:27 Eastern Standard Time (EST)[1]
Flight:	US Airways Flight 1549
Aircraft:	Airbus A320-214, Registration N106US
NTSB#:	DCA09MA026

B. GROUP

Chairman: John O'Callaghan
National Resource Specialist - Aircraft Performance
National Transportation Safety Board (NTSB)
490 L'Enfant Plaza E, SW
Washington, DC 20594

Members: N/A

C. SUMMARY

On January 15, 2009, about 15:27 eastern standard time, US Airways flight 1549, an Airbus A320-214, registration N106US, suffered bird ingestion into both engines, lost engine thrust, and landed in the Hudson River following take off from New York City's La Guardia Airport (LGA). The scheduled, domestic passenger flight, operated under the provisions of Title 14 CFR Part 121, was en route to Charlotte Douglas International Airport (CLT) in Charlotte, North Carolina. The 150 passengers and 5 crewmembers evacuated the airplane successfully. One flight attendant and four passengers were seriously injured.

This Aircraft Performance Study presents an analysis of the motion of the aircraft (specifically, a calculation of the aircraft position and orientation throughout the flight) based on the following information:

[1] All times are eastern standard time (EST) based on a 24-hour clock, unless otherwise noted.

- Touchdown location based on surveillance video
- Airport Surveillance Radar (ASR) data
- Flight Data Recorder (FDR) data
- Cockpit Voice Recorder (CVR) information
- Weather information

The study introduces the aircraft motion data collected during the investigation, describes the methods used to extract additional aircraft motion information from FDR, radar, CVR, and weather data, and presents the results of these calculations.

D. DETAILS OF THE INVESTIGATION

I. Touchdown location based on surveillance video

Reference 1 contains an analysis of a video clip from a surveillance camera located on the roof of Pier 88 in New York, performed by the Bureau d'Enquêtes et d'Analyses (BEA) of France. The clip depicts a nearly complete view of the landing of flight 1549 in the Hudson.

The results of BEA's analysis are shown in Figure 1. The blue line represents the path of the airplane through the water, from the touchdown point (labeled "Toucher queue") to the point where the airplane's speed through the water is zero (labeled "Immobilisation.") Reference 1 does not specify a latitude or longitude for these two points, but these coordinates can be estimated based on the satellite image in Figure 1 as follows:

"Toucher queue" (touchdown): N 40° 46' 16.78", W 074° 00' 20.50"
"Immobilisation" (stop): N 40° 46' 10.71", W 074° 00' 24.54"

II. Radar Data

Description of Radar Sites That Tracked US1549

In general, two types of radar are used to provide position and track information, both for aircraft cruising at high altitudes between airport terminal airspaces, and those operating at low altitude and speeds within terminal airspaces.

Air Route Surveillance Radars (ARSRs) are long range (250 nmi) radars used to track aircraft cruising between terminal airspaces. ARSR antennas rotate at 5 to 6 RPM, resulting in a radar return every 10 to 12 seconds. Airport Surveillance Radars (ASRs) are short range (60 NM) radars used to provide air traffic control services in terminal areas. ASR antennas rotate at about 13 RPM, resulting in a radar return about every 4.6 seconds. The FAA ASR-9 radars at Kennedy (JFK) and Newark (EWR) received returns from US1549. The data from the EWR ASR are presented in this Study.

Primary and Secondary Radar Returns

A radar detects the position of an object by broadcasting an electronic signal that is reflected by the object and returned to the radar antenna. These reflected signals are called *primary returns.* Knowing the speed of the radar signal and the time interval between when the signal was broadcast and when it was returned, the distance, or range, from the radar antenna to the reflecting object can be determined. Knowing the direction the radar antenna was pointing when the signal was broadcast, the direction (or bearing, or azimuth) from the radar to the object can be determined. Range and azimuth from the radar to the object define the object's position. In general, primary returns are not used to measure the altitude of sensed objects, though some ARSRs do have height estimation capability. ASRs do not have height estimation capabilities.

The strength or quality of the return signal from the object depends on many factors, including the range to the object, the object's size and shape, and atmospheric conditions. In addition, any object in the path of the radar beam can potentially return a signal, and a reflected signal contains no information about the identity of the object that reflected it. These difficulties make distinguishing individual aircraft from each other and other objects (e.g., flocks of birds) based on primary returns alone unreliable and uncertain.

To improve the consistency and reliability of radar returns, aircraft are equipped with transponders that sense beacon interrogator signals broadcast from radar sites, and in turn broadcast a response signal. Thus, even if the radar site is unable to sense a weak reflected signal (primary return), it will sense the response signal broadcast by the transponder and be able to determine the aircraft position. The response signal can also contain additional information, such as the identifying "beacon code" for the aircraft, and the aircraft's pressure altitude (also called "Mode C" altitude). The beacon code identifier for US1549 was 7134. Transponder signals received by the radar site are called *secondary returns*.

Recorded Radar Data

Recorded data from the EWR ASR was obtained from the FAA, and includes the following parameters:

- UTC time of the radar return, in hours, minutes, and seconds. EST = UTC – 5 hours.
- Transponder beacon code associated with the return (secondary returns only)
- Transponder reported altitude in hundreds of feet associated with the return (secondary returns only). The transponder reports pressure altitude. The altitude recorded in the file depends on the site recording the data; some sites record both pressure altitude, and pressure altitude adjusted for altimeter setting (MSL altitude). Others record just the adjusted altitude. The EWR file contains both altitudes, with the MSL altitude being 200 ft higher than the pressure altitude. The resolution of this data is ± 50 ft.
- Slant Range from the radar antenna to the return, in nmi. The accuracy of this data is ±1/16 nmi or about ± 380 ft.
- Azimuth relative to magnetic north from the radar antenna to the return[2]. The OKC ASR azimuth is reported in Azimuth Change Pulses (ACPs). ACP values range from 0 to

[2] The magnetic variation used by the EWR ASR to determine magnetic azimuth is 13° W.

4096, where 0 = 0° magnetic and 4096 = 360° magnetic. Thus, the azimuth to the target in degrees would be:

(Azimuth in degrees) = (360/4096) x (Azimuth in ACPs) = (0.08789) x (Azimuth in ACPs)

The accuracy of azimuth data is ± 2 ACP or ± 0.176º.

To determine the latitude and longitude of radar returns from the range and azimuth data recorded by the radar, the geographic location of the radar antenna must be known. The coordinates of the EWR ASR antenna are:

40° 40' 23.61" N latitude; 074° 11' 08.69" W longitude; elevation 3.9 feet

Presentation of the Radar Data

The data listed above for the EWR ASR-9 are presented in Tables 1a and 1b, and graphically in Figures 2-5. All the secondary returns recorded for US1549 are presented, but only those primary returns near the time and location of the bird-strike are presented.

In addition to the data recorded in file provided by the FAA, Tables 1a and 1b present several parameters derived using the recorded radar data and radar site location information, including the latitude and longitude of the radar returns, and the East and North coordinates of the returns relative to the LGA runway 4 threshold. Section D-III presents the relationship between the recorded radar time and the Flight Data Recorder (FDR) time. Range and azimuth data is converted into latitude and longitude and East and North coordinates using the WGS84 ellipsoid model of the Earth.

Figures 2 and 3 show the EWR ASR data plotted in terms of nautical miles north and east of the LGA runway 4 threshold. Figure 2 shows the data with a Cartesian grid background, and Figure 3 shows the data with a Google Earth satellite image background. The location, time, and altitude of the occurrence of selected CVR comments and sounds are also presented in Figures 2 and 3. Other position information, based on FDR data, is also shown in these Figures, and will be described in Section D-IV.

The north and east positions of the EWR ASR primary and beacon code 7134 returns are shown as a function of time in Figures 4a and 4b, along with other FDR-based data. Figure 4a shows data for the whole flight, and Figure 4b shows detail near the end of the flight.

The altitude of the airplane, as determined from the Mode C transponder returns, is shown as a function of time in Figures 5a and 5b, along with FDR-based altitude data. There is no altitude data for primary returns. The altitude data shown in Figures 5a-5b was used to correlate the radar and FDR clocks, as described in Section D-III.

III. Flight Data Recorder (FDR) and Cockpit Voice Recorder (CVR) Data

FDR and CVR Data Description

The aircraft cockpit voice recorder (CVR) and flight data recorder (FDR) were recovered from the aircraft and sent to Washington, DC for readout.

Descriptions of the FDR and CVR and the recorder readout processes can be found in References 2 and 3, respectively. The FDR readout results in tabulated and plotted values of the recorded flight parameters versus time. The CVR readout results in a transcript of the CVR events, a partial list of which is shown in Table 2. The selected CVR events listed in Table 2 are also presented along with other information in Figures 2 and 3. For the complete list of CVR events, see Reference 3.

Correlation of Radar, FDR, and CVR Times

The ASR-9 radar, the FDR, and the CVR record their information with respect to time, but these recorded times are not synchronized. To use these data sources together, their times must be synchronized to a single reference time. This reference time is the EWR ASR EST time introduced in Section D-II and used throughout this Study.

Time on the FDR is measured in terms of the Subframe Reference Number (SRN), with one SRN equivalent to one second of time.

The relationship between the time recorded by the EWR ASR-9 radar and the FDR SRN is established by comparing the altitude recorded by the FDR with the Mode C altitude recorded by the radar (uncorrected for altimeter setting). Both altitudes are based on the static pressure sensed at the airplane's static pressure ports, and on a sea level pressure of 29.92 "Hg (i.e., both altitudes are pressure altitude). By adjusting the FDR times so that the FDR altitude falls within the ±50 ft. uncertainty band of the EWR Mode C altitude throughout the flight, the offset between the FDR SRN and radar time can be determined.

This process is illustrated in Figure 5a, and gives the result

15:00:00 (EST) EWR ASR-9 Radar Time = 63701.119 FDR SRN [1]

The relationship between the times of events recorded on the CVR and the EWR ASR-9 reference time is established by first establishing the conversion from CVR to FDR time, and then using the FDR to EWR ASR-9 time conversion defined by Equation [1]. The correlation between the FDR and CVR times is described in Reference 3. The CVR transcript provided in Reference 3 uses the EWR ASR-9 times, and selected events from the transcript are presented in Table 2 and Figures 2 and 3.

The "sound of thump/thud(s) followed by shuddering sound" recorded by the CVR at 15:27:11.40 is most likely the result of the bird-strike. This event is depicted on various Figures that plot data vs. time as a vertical line located at time 15:27:11.40.

IV. Performance Calculations based on FDR Data

Overview

The FDR records many, but not all, performance parameters of interest. Many additional parameters can be derived from the FDR parameters; however, the FDR parameters themselves can suffer from inherent measurement errors[3] and must be corrected before being used in these calculations.

This section describes the corrections applied to the FDR data, and the calculations used to derive additional performance parameters from the corrected data. The airplane weight used in these calculations is 151,000 lb.[4] Further details on the derivation of the equations and calculation methods used in this Study can be found in Appendix A of Reference 4.

The FDR corrections discussed in this Study attempt to remove the following errors:

- Altitude error associated with non-standard day conditions (pressure altitude to actual altitude estimate)
- Altitude sampling time error associated with the update and sample rate of altitude data
- Accelerometer bias errors
- Errors in recorded groundspeed and drift angle that result in a ground track that differs slightly from the recorded GPS-based track

The performance parameters derived from the corrected FDR data include:

- True airspeed
- True altitude and density altitude
- Static temperature
- Groundspeed and drift angle "calibrated" to match GPS track
- Airplane positions and velocities from accelerometer integration
- Flight path angle (γ)
- Angle of attack (α) and sideslip angle (β)
- Wind speed and direction

The results of these corrections and derivations are presented in Figures 4-13. The "a" Figures present the results for the entire flight; the "b" Figures show the last 75 seconds of the FDR data in more detail. In what follows, a reference to a Figure number refers to both the "a" and "b" Figures, unless the "a" or "b" is explicit in the reference. Thus, for example, "Figure 10" refers to both Figures 10a and 10b, but "Figure 10a" refers only to that Figure.

[3] "Measurement error" in this context means the difference between the actual true value of the quantity being measured and the measured or recorded value. It does not necessarily imply defects or malfunctions in the measurement and recording equipment itself. This difference can result from, among other things, limitations in the sensor accuracy and / or resolution.

[4] This value was provided by the Operations Group. The gross weight recorded on the FDR was 151760 lb at takeoff, and 150800 lb at touchdown.

Correction of the sample times of altitude data

Computing rate of climb based on the time derivative of the pressure altitude recorded by the FDR results in an unrealistic "square wave" oscillation about the likely true value of rate of climb. The period of this oscillation is about 4 seconds. The source of the oscillation is also apparent in the pressure altitude data itself, which during the climb appears to "step" every fourth data point (see Figure 5c).

According to the Airbus FDR Group Member, this behavior is a result of the difference between the update rate of the altitude data in the Display Management Computer (DMC), which is once every 0.8 seconds, and the recording or sampling rate of the FDR, which is once every second. As a consequence of this difference, one out of every 5 DMC altitude samples is omitted from the FDR recording.

It should also be noted that the recording architecture does not necessarily guarantee that the sampling time associated with a recorded altitude value does in fact correspond to the time the value was sensed. In this case, the data values associated with a given sample time may in fact be up to 0.8 seconds old.

The behavior of the recorded altitude (and corresponding rate of climb) can be made more realistic by "correcting" the recorded sample times to reflect the actual 0.8 second update interval of the DMC, and the "missing" sample every 5^{th} point. To accomplish this, the time interval between successive points is forced to equal to the DMC update interval (0.8 seconds), except that the time interval between every 4^{th} and 5^{th} point is forced to equal twice the update interval (i.e., 1.6 seconds).

The results of this correction are shown in Figure 5c as the altitude and rate of climb corresponding to the "Corrected sample times." As shown in the Figure, the "stepping" behavior of the altitude data is removed, and the missing data point every 4 seconds is apparent. The "square wave" oscillation in the rate of climb calculation has also been eliminated.

The calculations described below that use the FDR pressure altitude data are based on the data with the corrected sample times.

True airspeed calculation

True airspeed equals the Mach number multiplied by the speed of sound; the speed of sound is a function of the static temperature. Static temperature is obtained from total temperature and Mach number.

Mach number can be computed from calibrated airspeed and static pressure. Total temperature and calibrated airspeed are recorded directly by the FDR, and the static pressure can be determined from the pressure altitude recorded by the FDR (which is based on the standard sea-level pressure of 29.92 "Hg).

Figure 6 shows the results of the true airspeed calculation, compared with the indicated (calibrated) airspeed recorded by the FDR. Figure 6 also shows the groundspeed recorded by the FDR, and the groundspeed obtained from integration of the accelerometer data (this calculation is described below).

Pressure-based true altitude and density altitude calculations

The altitude recorded by the FDR is pressure altitude (i.e., the altitude in the standard atmosphere corresponding to the static pressure sensed at the airplane's static port). The altimeter setting at the time of the accident was 30.25 "Hg[5], and so actual MSL altitude is about 305 ft higher than pressure altitude. However, the pressure altitude adjusted for altimeter setting alone may not necessarily match the true MSL altitude throughout the flight because, in general, the lapse rate of pressure with altitude does not match the lapse rate in the standard atmosphere.

To estimate the actual altitude of US1549, the change in altitude corresponding to a change in static pressure is calculated by solving the hydrostatic equation continuously (the hydrostatic equation describes the pressure increment across a differential element of air required to balance the weight of the element; see Appendix A of Reference 4). With static pressure and the static temperature values from the speed calculations, the density and weight of the air elements can be calculated.

The results of this calculation are shown in Figure 5 as the line labeled "Altitude based on hydrostatic equation." The density altitude is the altitude in the standard atmosphere corresponding to the actual air density at each point in the flight. Because of the colder-than-standard day, the density altitude throughout the flight was about 3000 ft lower than the true MSL altitude.

The calculated static temperature is shown in the bottom graph of Figure 12, along with the total temperature recorded by the FDR.

Flight path angle (γ), angle of attack (α), and sideslip angle (β) calculations

The flight path angle is defined by

$$\gamma = \sin^{-1}\left(\frac{\dot{h}}{V}\right) \qquad [2]$$

where γ is the flight path angle, $\dot{h}$ is the rate of climb, and V is speed. The γ relative to the airmass resulting from using $\dot{h}$ and V from the true altitude[6] and true airspeed calculations described above in Equation [2] is shown in Figure 7 as the gray line. The γ relative to the Earth resulting from using $\dot{h}$ and V from integrated accelerometer data is shown in Figure 7 as the red line (the accelerometer integration method is described below).

The sideslip angle (β) is the angle that the velocity vector of the airplane relative to the airmass makes with the airplane's plane of symmetry (see Figure 8). This angle is required to resolve the airspeed of the airplane into components along each of the airplanes axes, which in turn is required to estimate the atmospheric wind from the FDR data. Consequently, the behavior of β during the flight is of interest.

[5] This is the altimeter setting at LGA from the METAR report closest to the time of the accident (15:51 EST). The altimeter setting used by the flight crew was that current for LGA during the departure (30.23" Hg).
[6] Throughout the remainder of this Study, "true altitude" refers to the "Altitude based on hydrostatic equation" altitude shown in Figure 5.

β is not sensed or recorded by the FDR, and so must be calculated from other parameters. An estimate of β can be made if the side force (Y) characteristics of the airplane are known and if the side force generated during the flight can be calculated. The most significant contributors to the side force are β and rudder deflection (δr):

$$C_Y = \frac{Y}{\frac{1}{2}\rho V^2 S} = \frac{\partial C_Y}{\partial \beta}\beta + \frac{\partial C_Y}{\partial \delta r}\delta r + \{\text{smaller terms}\} \qquad [3]$$

Where C_Y is the side force coefficient, ρ is the air density, V is true airspeed, and S is the wing reference area (1319.7 ft^2). Ignoring the smaller terms, Equation [3] can be solved for an estimate of β:

$$\beta \cong \frac{C_Y - \frac{\partial C_Y}{\partial \delta r}\delta r}{\frac{\partial C_Y}{\partial \beta}} \qquad [4]$$

The derivatives $\partial C_Y / \partial \beta$ and $\partial C_Y / \partial \delta r$ are aerodynamic characteristics of the airplane. Airbus declined to provide the value of these terms to the NTSB[7], and so for this Study the values were estimated based on known values for an airplane of similar configuration.

The side force Y can be calculated using

$$Y = (W)(n_y) \qquad [5]$$

Where W is the weight of the airplane and n_y is the lateral load factor recorded by the FDR.

The β computed using Equation [4] is shown in Figure 9 as the gray line labeled "Sideslip angle from aero coefficient buildup."

Once γ and β are computed, they can be used along with the pitch angle (θ) and roll angle (ϕ) recorded by the FDR to compute the angle of attack, α:

$$\alpha = \tan^{-1}\left(\frac{\tan\theta}{\cos\phi}\right) - \sin^{-1}\left(\frac{\sin\gamma + \sin\beta\cos\theta\sin\phi}{\cos\beta\sqrt{1-\cos^2\theta\sin^2\phi}}\right) \qquad [6]$$

Note that when $\beta = \phi = 0$, Equation [6] simplifies to the well-known result that $\alpha = \theta - \gamma$. The α resulting from Equation [6] is shown in Figure 7 as the gray line labeled "Based on pressure altitude and airspeed." The α resulting from the components of airspeed along each of the airplane's axes, as determined from integrated accelerometer data and computed winds, is shown in Figure 7 as the red line labeled "Based on accelerometer

[7] Airbus offered to present and discuss the aerodynamic characteristics of the airplane, and perform simulations or other calculations with the NTSB Aircraft Performance Group Chairman, on-site at Airbus facilities in Toulouse, but declined to provide the values of $\partial C_Y / \partial \beta$ and $\partial C_Y / \partial \delta r$ outside of this context.

integration and winds" (the accelerometer integration method is described below). The θ and ϕ recorded by the FDR are shown in Figures 7 and 9, respectively.

The angles of attack based on the left and right α-vane measurements recorded on the FDR are also shown in Figure 7. True α was computed from the vane measurements using calibration equations provided by Airbus.

Accelerometer data corrections and integration

The accuracy of the calculations that use the FDR altitude and airspeed data as inputs are limited by the accuracy and sample rate of that data. In particular, the rate of climb – and consequently, the γ and α – that are computed using the pressure-based altitude data will be "noisy" (see the "Based on pressure data" result in Figure 6, and the resulting γ and α in Figure 7).

A more accurate calculation of the flight path of the airplane during relatively short intervals (about 30 to 60 seconds) can be obtained by integrating the accelerations recorded at the CG of the airplane. However, the accelerometers are generally not located exactly on the CG, and so the accelerations at the CG must be computed by adjusting the FDR-recorded load factors for the effects of angular rates and accelerations. Furthermore, accelerometers generally contain small offsets, or "biases," that produce large errors in speed and position if not removed prior to integration[8]. In addition, the initial values of speed, rate of climb, and track angle are required during the integration process (these are essentially the "constants of integration" when integrating acceleration to get speeds). The constants of integration and the values of the accelerometer biases can be estimated by selecting them such that the aircraft position that results from the integration agrees with known positions determined from another source. In this Study, the "target" positions are those defined by an integration of the groundspeed and drift angle data recorded by the FDR, and the true altitude shown in Figure 5, adjusted to match the FDR radar altitude at the start and end of the flight.

Accelerations at the CG

The accelerations at the CG can be computed from the load factors recorded by the FDR as follows. The acceleration at any point P on the airplane, $\vec{a}_P$, is given by

$$\vec{a}_P = \begin{Bmatrix} \dot{u} + wQ - vR \\ \dot{v} + uR - wP \\ \dot{w} + vP - uQ \end{Bmatrix} + \begin{Bmatrix} Q(yP - xQ) + R(zP - xR) + (z\dot{Q} - y\dot{R}) \\ R(zQ - yR) + P(xQ - yP) + (x\dot{R} - z\dot{P}) \\ P(xR - zP) + Q(yR - zQ) + (y\dot{P} - x\dot{Q}) \end{Bmatrix} = \vec{a}_{CG} + \Delta\vec{a} \qquad [7]$$

where:

$\{u, v, w\}$ = components of inertial velocity in the airplane body axes
$\{P, Q, R\}$ = components of angular velocity in the airplane body axes
$\{\dot{P}, \dot{Q}, \dot{R}\}$ = time derivatives of $\{P, Q, R\}$
$\{x, y, z\}$ = coordinates of point P in the airplane body axes

[8] For details about the equations to be integrated and the bias correction technique described in this Study, see Appendix A of Reference 4.

(see Figure 8). Since by definition {x, y, z} at the CG = {0,0, 0}, the first term in brackets in Equation [7] is the acceleration of the CG ($\vec{a}_{CG}$), and the second term is the increment in acceleration due to the point P being away from the CG ($\Delta\vec{a}$).

A three axis accelerometer at point P will measure load factors as follows:

$$\vec{n}_P = \frac{\vec{a}_P - \vec{g}}{g} = \frac{\vec{a}_{CG} + \Delta\vec{a} - \vec{g}}{g} = \vec{n}_{CG} + \frac{\Delta\vec{a}}{g} \qquad [8]$$

Where $\vec{g}$ is the gravity vector, g is the acceleration due to gravity (32.17 ft/s^2), and Equation [7] has been used to substitute for $\vec{a}_P$. The components of $\vec{n}$ are {n_x, n_y, n_z}. The normal load factor (*nlf*) is

$$nlf = -n_z \qquad [9]$$

The FDR records n_x, n_y, and *nlf* as "Longitudinal Acceleration," "Lateral Acceleration," and "Vertical Acceleration." The values of {n_x, n_y, n_z} at the CG can be found using the FDR data and Equations [9], [8], and [7], with {x y, z} in [7] being the distance of the accelerometer unit from the CG.

The angular rates and accelerations used to evaluate Equation [7] are computed from the θ and ϕ angles recorded by the FDR, and true heading (ψ_T). The ψ_T is based on the magnetic heading (ψ_M) recorded by the FDR[9]. ψ_M and ψ_T are presented in Figure 9.

The angular rates and accelerations throughout the flight were very small. This fact, together with the relatively close proximity of the accelerometers to the CG, make the $\Delta\vec{a}$ defined in Equation [7] negligibly small, and so in this case the {n_x, n_y, n_z} recorded by the accelerometers are good measures of the {n_x, n_y, n_z} at the CG. However, these data must still be corrected for accelerometer bias.

Accelerometer bias calculations

The accelerometer biases are not necessarily constant over an entire flight, but can drift over time. It is for this reason that integrating the accelerometers works best over relatively short intervals, during which the accelerometer biases are approximately constant. In order to obtain an integrated flight path for the entire accident flight, the flight was divided into five segments, and the accelerometer data was integrated separately for each segment. In each of these segments, the constants of integration and the accelerometer biases were chosen to minimize the difference between the integrated north and east position and the north and east position obtained from an integration of the FDR groundspeed and drift angle data, and the difference between the integrated altitude and the "Hydrostatic altitude adjusted to match radio altitude" data shown in Figure 5.

For each segment, the constants of integration (the initial groundspeed, track angle, and rate of climb) are chosen to minimize the root-mean-square difference between the integrated flight path and the target flight path throughout the entire segment. The accelerometer biases are chosen to minimize the error between the integration and the

[9] True heading is computed assuming a magnetic variation of 13° west (i.e., $\psi_T = \psi_M$ - 13°).

target at the end point of the integration; i.e., the biases are chosen so that the integrated flight path and target flight path coincide at the end of each segment. The beginning and end times, constants of integration, and accelerometer biases used for the five segments are shown in Table 3. The constants of integration are expressed as increments, or biases, on the initial groundspeed, track, and rate of climb that would be computed using the target trajectory.

The integration of the FDR groundspeed and drift angle data, which serves as the "target" for the integration of the accelerometer data, also requires some correction. This is because the track produced by integrating the FDR groundspeed and drift angle (without adjustment) differs slightly from the track recorded in the FDR GPS position data[10].

To ensure that the integration of groundspeed and drift angle match the GPS track over the length of each segment, a time-weighted velocity vector is added to the north and east velocities defined by the FDR groundspeed and drift angle. This vector then forces the integration of the north and east velocities to match the GPS position at a point near the end of the segment. The vector can be thought of as a "wind," with a velocity and direction, that "blows" the airplane onto the GPS position at the specified time.

The time-weighted "shape" of the velocity vector is shown in Figure 10. The magnitude of the vector is multiplied by the factor k in this Figure, which changes over the length of the integration. At the beginning and end of the integration, the value of k is 0.0, and so the corrected east and north velocities match those defined by the FDR groundspeed and drift angle data at these points. The k factor ramps up to 1.0 over the first third of the segment, remains at 1.0 over the second third, and ramps back to 0.0 over the last third.

The values of the velocity vectors for each integration segment, expressed as wind velocities and directions, are listed in Table 3.

The north and east positions, and MSL altitude, resulting from the accelerometer integrations (not the groundspeed/drift angle integration) are shown in Figures 3-5.

Wind calculations

Airspeed, groundspeed, and wind are related as follows:

$$\vec{V}_W = \vec{V}_G - \vec{V} \qquad [10]$$

where $\vec{V}$ is the airspeed vector, $\vec{V}_G$ is the groundspeed vector and $\vec{V}_W$ is the wind vector (see Figure 11). The components of $\vec{V}_G$ in body axes result from the integration of the accelerometer data described above. The components of the airspeed $\vec{V}$ in body axes, as indicated by Figure 8, are related to α and β as follows:

[10] The GPS provides a reliable measure of the absolute position of the airplane throughout the flight; however, speeds and track angles computed from the GPS data are more "noisy" than the inertial groundspeed and drift angle recorded by the FDR. To obtain a smooth "target" track for the accelerometer integration, the integrated groundspeed and drift angle track is preferred to the GPS track. However, since the GPS track, while noisier, provides a better measure of the "absolute" position of the airplane over long periods, the groundspeed / drift angle integration must be adjusted to prevent it from diverging from the GPS track over time.

$$u = V\cos(\beta)\cos(\alpha) \quad [11a]$$
$$v = V\sin(\beta) \quad [11b]$$
$$w = V\cos(\beta)\sin(\alpha) \quad [11c]$$

where β and α are computed using Equations [4] and [6], respectively. Once the components of $\vec{V}_W$ in the airplane body axes are computed using Equation [10], they can be transformed into Earth axes using the known θ, ϕ, and ψ_T. The results of the wind calculations are shown in Figure 12 as a function of time, and in Figure 13 as a function of altitude. The "Fit to computed winds" lines shown in Figure 13 provide a "smoothed" wind profile as a function of altitude, which can be used to compute inertial α, β, and γ values.

Inertial γ, α, and β calculations

A second method of calculating α and β involves computing the airplane's airspeed components along each of the body coordinate axes, using the known inertial speed components resulting from the accelerometer integration, the "smoothed" winds shown in Figure 13, and Equation [10]. This method assumes that the winds are not really as "noisy" as the computed winds shown in Figures 12 and 13. Furthermore, the method assumes zero vertical wind[11]. Since the integrated inertial velocities are smooth, and the winds are smooth, the α and β computed from these quantities are also relatively smooth (compare the inertial α and β calculations with the other α and β calculations in Figures 7 and 9).

From Figure 8, we see that

$$\alpha = \tan^{-1}\left(\frac{w}{u}\right) \quad [12]$$
$$\beta = \sin^{-1}\left(\frac{v}{V}\right) \quad [13]$$

where V is total airspeed, and $\{u, v, w\}$ are the components of airspeed in body axes. Per Equation [10], the airspeed and its components in the body axes can be computed if the components of both the groundspeed and wind speed are known. The components of $\vec{V}_G$ in body axes result from the integration of the accelerometer data described above. The components of $\vec{V}_W$ can be calculated by transforming the components of the smoothed wind in Earth axes into body axis using the recorded Euler angles (θ, ϕ, and ψ_T).

The results of the inertial α and β calculations are shown in Figures 7 and 9 as the red lines. Note that the results agree well with the α and β computed using Equations [6] and [4], respectively, but are much smoother.

The inertial γ shown in Figure 7 is computed using Equation [2], with $\dot{h}$ and V from the integrated accelerometer data described above. For this calculation, V is the total inertial speed relative to Earth (not airspeed), so the inertial γ is also relative to Earth. Using V from Equation [10] (airspeed), γ is relative to the air (about 0.1º higher than γ relative to Earth).

[11] The wind calculation described above also yields values for the vertical wind. The computed vertical wind oscillates noisily about 0 throughout the flight, and is not plotted in this Study.

V. Additional FDR Data Related to Aircraft Performance

Other parameters recorded by the FDR that are relevant to aircraft performance include the cockpit controls (throttle, longitudinal and lateral side stick positions, and rudder pedal position), the aerodynamic control surfaces (elevators, ailerons, spoilers, and rudder), the engine speeds, and the airplane configuration (flap and gear position). The recorded data is presented in Figures 14-17 as follows:

Figure 14 – Controls (sidestick and rudder pedal and rudder surface positions)
Figure 15 – Control surfaces (elevators, ailerons, and spoilers)
Figure 16 – Power (throttle positions and engine N1 and N2 speeds)
Figure 17 – Configuration (flaps, slats, and gear positions)

VI. Flight Envelope Protection Information

A320 flight control laws and flight envelope protection features

The Airbus A320 is a "fly-by-wire" airplane in the pitch and roll axes, meaning that pilot control inputs on the sidestick controllers are processed by a flight control computer, which then sends electrical signals to the actuators that move the flight control surfaces (ailerons, spoilers, and elevators). Directional control through the rudder is not fly-by-wire; the rudder actuators are linked mechanically by cables to the rudder pedals in the cockpit, though a yaw damper provides additional rudder inputs in parallel with the rudder pedals.

In the pitch and roll axes, the fly-by-wire design allows for "envelope protection." The flight control computers monitor the pitch and roll states of the airplane, and intervene to prevent departures from controlled flight. According to a presentation given by an Airbus test pilot at the Public Hearing for this accident (Reference 5), the high angle-of-attack element of the fly-by-wire envelope protection[12]:

- Provides positive static stability at the low speed end of the flight envelope
- Protects against stall, even in high dynamic maneuvers or in turbulent or gusty conditions
- Provides the ability to reach and maintain a high lift coefficient, with full aft sidestick, without exceeding the stall angle of attack

Additionally, the envelope protection when α-protection is active:

- Limits the load factor of the airplane
- Limits the bank angle to 45°
- Freezes the pitch trim in nose-high attitudes
- Is available from lift-off to landing

Reference 6, the Airbus Flight Crew Training Manual (FCTM), further describes the "fly-by-wire" control laws and the high-angle-of-attack envelope protection afforded by these laws:

[12] In the discussion that follows, the high angle-of-attack element of the fly-by-wire envelope protection is referred to as "α-protection."

> The relationship between the Pilot Flying's (PF's) input on the sidestick, and the aircraft's response, is referred to as control law. This relationship determines the handling characteristics of the aircraft. There are three sets of control laws, and they are provided according to the status of the: Computers, peripherals, and hydraulic generation.
>
> The three sets of control laws are:
>
> • Normal law
> • Alternate law
> • Direct law.
>
> …
>
> Under normal law, when the angle of attack becomes greater than α_{prot}, the system switches elevator control from normal mode to a protection mode, in which the angle of attack is proportional to sidestick deflection. That is, in the α_{prot} range, from α_{prot} to α_{max} the sidestick commands α directly. However, the angle of attack will not exceed α_{max}, even if the pilot gently pulls the sidestick all the way back. If the pilot releases the sidestick, the angle of attack returns to α_{prot} and stays there.

According to discrete parameters recorded on the FDR, US1549 remained in Normal Law throughout the flight, and so the high-angle-of-attack envelope protection described in the FCTM would have been available.

α, α_{prot}, and α_{max} relationships during the descent

Reference 7 describes simulation studies done in support of the US1549 investigation in crew training and engineering simulators at Airbus facilities in Toulouse[13]. Recorded data from the engineering simulator includes parameters containing the values of α_{prot} and α_{max} at each point in the simulation. Together with configuration information recorded by the simulator, these parameters provide an indication of the values of α_{prot} and α_{max} as a function of flap and slat settings. The data indicates that the value of α_{prot} steps up 1° as the airplane nears the ground without a change in configuration. Airbus confirms that this step occurs within 1 second as the airplane descends through of 50 ft radio altitude. Based on these observations, the definition of the values of α_{prot} and α_{max} were estimated to depend on the airplane configuration and radio altitude as follows:

$$\alpha_{prot} = 8° + (0.36111)*\min(\delta_{slats}, 18.0°) \quad [14a]$$

$$\text{If } \delta_{slats} > 17° \text{ and } h_{radio} <= 50 \text{ ft. then } \alpha_{prot} = 15.5° \quad [14b]$$

$$\alpha_{max} = 11° + (0.36111)*\min(\delta_{slats}, 18.0°) \quad [15]$$

Where δ_{slats} is the slats position in degrees, and h_{radio} is the radio altitude. The function $\min(\delta_{slats}, 18.0°)$ indicates that the lesser value of δ_{slats} or 18.0° is to be used in the equation.

The values of α_{prot} and α_{max} defined by Equations [14a], [14b], and [15] are plotted in Figure 7. The Figure shows that α is greater than α_{prot} between 15:27:35 and 15:28:10, and that α oscillates about ±1°above and below α_{prot} between 15:29:05 and 15:29:48. At 15:29:48, as

[13] The simulations included normal landings, ditching maneuvers at various flap settings, and evaluations of the energy available to glide to a landing at LGA or Teterboro, NJ (TEB) following the birdstrike. See Reference 7 for detailed descriptions of these maneuvers and the simulation results.

the flaps extend to conf2, α_{prot} ramps up from 8° to 14.5°, and α_{max} ramps up from 11° to 17.5°. Between 15:29:48 and 15:30:32, α is less than α_{prot}; between 15:30:32 and 15:30:39, the inertial-based α oscillates between 13.5° and 15°, i.e., above and below α_{prot}. At 15:30:39, as the airplane descends through 50 ft radio altitude, α_{prot} increases to 15.5° while α remains at about 13.5° to 14.5°, or about 1.5° below α_{prot} and about 3.5° below α_{max}.

Pitch angle behavior in the 100 ft prior to touchdown

The pitch angle behavior of the airplane in the last 100 ft of flight is of interest, since changes in pitch have a strong influence on the flare and touchdown conditions. As noted above, in the last 50 ft, the angle of attack was about 3.5° below α_{max} and even 1.5° below α_{prot}; consequently, there was some additional angle of attack margin available to flare the airplane and reduce the descent rate at touchdown. Starting at about 15:30:36, at a radio altitude of about 100 ft, the FDR records a progressive pull on the left longitudinal side stick, with a momentarily relaxation from 5° to 3° at 15:30:37, returning to 7° at about 15:30:38. At 15:30:39, as the airplane descends through 50 ft, the stick moves aft more abruptly, reaching its aft limit (16°) at about 15:30:41, and remaining there about 2 seconds, until touchdown at 15:30:43.

The elevator response plotted in Figure 15b indicates that during this time, the elevators move trailing-edge up starting at 15:30:37, reaching about 4° at 15:30:38, and then move abruptly down to about -1° at 15:30:39 before increasing again to about 4.5° at 15:30:41. In the last 2 seconds of flight, the elevator deflection increases about 1°, from 4.5° to 5.5°.

Figure 7 shows that between 15:30:36 and the touchdown at 15:30:43, the pitch angle increases from 9.5° to 11° and then settles back to 9.5°, even though in the last two seconds the left longitudinal side stick is at its aft limit, and α is below α_{max}.

Reference 8 documents an Airbus simulation of the last 300 ft of the flight, and indicates that the airplane was performing as designed as was in α-protection mode from 150 ft to touchdown. Per Reference 6 (quoted above), in α-protection mode, “the angle of attack is proportional to side stick deflection. That is, in the α_{prot} range, from α_{prot} to α_{max} the side stick commands α directly” while keeping $\alpha < \alpha_{max}$. However, in α-protection mode, the flight control system incorporates a phugoid-damping feedback term in addition to side stick commands when computing the commanded elevator position (which in turn determines the pitch angle response). As described by Airbus,

> … the aircraft was in angle-of attack (AoA) protection from about 150 ft RA. When in AoA protection law, stick command is AoA objective. Stick neutral commands alpha-prot and full back stick commands alpha-max.
>
> However, AoA protection shall take care of the A/C trajectory and, thus, looks after phugoid damping as well as AoA control: there are feedbacks within the AoA protection law aiming at damping the phugoid mode (low frequency mode). The feedbacks are CAS and pitch attitude variations. Without these feedbacks, an aircraft upset from its stabilized flight point up to constant high AoA would enter a phugoid (which is, by definition, a constant AoA oscillation) without possibility to stabilize the trajectory. As a consequence, commanded AoA is modulated as a function of speed and attitude variations: for instance, if A/C speed is decreasing and/or pitch attitude is increasing, pilot's commanded AoA is lowered in order to avoid such a situation to degrade.
>
> On the last 10 sec of the "Hudson" event, it is confirmed that pitch attitude is increasing and CAS

> decreasing. Then, the phugoid damping terms are non nul and are acting in the sense to decrease the finally commanded AoA vs. the stick command, in order to prevent the aircraft from increasing the phugoid features.[14]

Based on this explanation, it appears that on the accident flight, the nose-up side stick commands from 15:30:36 to 15:30:43 were offset somewhat by the phugoid-damping feedback term, thereby limiting the pitch angle and α increase below 150 ft radio altitude.

As noted above, the simulation documented in Reference 8 indicates that the α-protection mode was active in the last 150 ft (or, from 15:30:33 and on), even though in the last 50 ft (15:30:39 and on) α is less than α_{prot}. This is so because while the α-protection mode is activated whenever α increases to or above α_{prot}, a drop in α below α_{prot} does not by itself de-activate the α-protection mode. As described by Airbus,

> The activation of the alpha protection law is mainly related to a comparison alpha vs alpha threshold.
>
> However, the de-activation of the alpha protection law is not only a matter of comparison alpha vs alpha prot threshold. The logic also takes into account the stick input and the "history" (was the aircraft in protection or not).
>
> If the law has been triggered, to phase it out, in the great lines, you need one of those conditions:
>
> - stick significantly pushed forward, without reference to AoA value
>
> or
>
> - stick slightly pushed forward + AoA not too far from alpha max
>
> or
>
> - stick not too aft + low AoA.
>
> In the Hudson event, none of those 3 conditions were achieved below 150 ft.[15]

Consequently, the α-protection mode remained active below 50 ft radio altitude, even though α was less than α_{prot}.

[14] Airbus email to the Aircraft Performance Group Chairman, dated October 5, 2009.
[15] Airbus email to the Aircraft Performance Group Chairman, dated November 18, 2009.

E. CONCLUSIONS

The video data, radar, FDR, and CVR data presented in this Study are consistent with the following sequence of events concerning the motion of US Airways Flight 1549:

The airplane started its takeoff roll from runway 4 at about 15:25:04, lifting off about 36 seconds later. Based on recorded sidestick controller inputs, the First Officer was the pilot flying. At 15:27:05, as the airplane was climbing through 2500 ft, the flaps were retracted, and about five seconds later, the Captain stated "birds." At 15:27:11.4, as the airplane was climbing through 2750 ft, and crossing a line of primary returns detected by the EWR ASR-9, the CVR recorded the "sound of thump/thud(s) followed by [a] shuddering sound." At the same time, the N1 speed of both engines dropped suddenly (to about 35% N1 on engine 1, and to about 15% N1 on engine 2). The n_x at this point dropped from about 0.22 G's to 0.05 G's, indicating a dramatic drop in acceleration. Concurrent with the drop in n_x, the airspeed immediately started decaying from its value of 219 KCAS at the time of the sound of the thumps. Based on the reports of the crew and the remains of Canada geese eventually found in the engines, the "thump" sounds and decay in engine N1 speeds recorded at 15:27:14 most likely resulted from the ingestion of Canada geese into the engines. Within 12 seconds of the bird-strike, the Captain took action to start the Auxiliary Power Unit and called "my aircraft." Recorded sidestick controller inputs indicated that he took over control of the airplane from the First Officer at about 15:27:24. At 15:27:28, the Captain called "get the QRH… loss of thrust on both engines."

Following the bird strike, the airplane's altitude continued to increase while the airspeed decayed, until 15:27:30, when the altitude peaked at about 3060 ft, at an airspeed of about 185 KCAS. At that point, the altitude started to decrease, as the airspeed started to increase, reaching 210 KCAS at about 15:28:10, at an altitude of 1650 ft.

At 15:27:25, the airplane started rolling into a left bank, and at 15:27:33, as the airplane was descending through 3020 ft, the Captain contacted ATC and declared an emergency, stating the flight needed to return to LGA. At 15:27:42 ATC instructed US1549 to turn left to a heading of 220°. The airplane continued its left turn and rolled out onto a heading of about 230° at 15:28:30, while descending through 1450 ft and decelerating through 200 KCAS. During the turn, the CVR recorded the crew working their way through the Quick Reference Handbook checklist for loss of thrust on both engines, and indicating to ATC that they would not be able to make LGA and might "end up in the Hudson." Over the next minute, the Captain and ATC discussed the possibility of a landing at Teterboro, but at 15:29:28, as the airplane was descending through 700 ft, the Captain stated "we're gonna be in the Hudson." At this point, the airplane was near the west shore of the Hudson river, and turned slightly left to track down the river.

Between 15:29:00 and 15:30:00, the airplane descended from 1200 ft to 200 ft, and the airspeed stabilized between 185 and 193 KCAS. At these speeds, the angle of attack ranged between 7° and 9°, bracketing the α_{prot} value of 8° for the flaps-up configuration at low Mach number.

At 15:29:49, as the airplane was descending through 270 ft, the flap handle was moved to conf2. As the flaps deployed, the airplane descended to about 210 ft and then climbed briefly, reaching 360 ft at 15:30:16, before descending again. At conf2, α_{prot} increased from 8° to 14.5°, and α_{max} increased from 11° to 17.5°. At 15:30:17 the First Officer asked the Captain, "got flaps two, you want more?" The Captain replied, "no, let's stay at two."[16]

Following the flap deployment at 15:29:49, and during the final descent to the water, the airspeed decayed from about 194 KCAS to 125 KCAS at touchdown. Simultaneously, the angle of attack increased from about 8° to about 13° or 14° at touchdown. A simulation performed by Airbus indicated that from about 150 ft radio altitude to touchdown, the airplane was in α-protection mode as a result of α reaching α_{prot}. As the airplane descended below 50 ft, α_{prot} increased from 14.5° to 15.5°, though the airplane remained in α-protection mode because the conditions to deactivate this mode were not satisfied. A phugoid damping feedback term in the flight control laws, that is active in α–protection mode, attenuated the airplane's nose-up pitch response to progressively larger aft side stick inputs made below 100 ft radio altitude.

The airplane touched down on the Hudson at 15:30:43, under the following conditions:

Airspeed (FDR):	125 KCAS
Groundspeed (computed):	126 knots
Rate of descent (computed):	-750 ft/min
γ (relative to Earth, computed):	-3.4°
γ (relative to airmass, computed):	-3.5°
θ (FDR):	9.5°
ϕ (FDR):	0.4°
α (computed):	12.9°
α (measured):	13.7° (left vane), 14.5° (right vane)
β (computed):	2.2°
Drift angle (computed):	-1.4°
Track angle (computed):	210.7° true
Heading angle (FDR):	209.9° true
Location (video):	N 40° 46' 16.78", W 074° 00' 20.50"

_____

John O'Callaghan
National Resource Specialist - Aircraft Performance
Office of Research and Engineering

[16] The US Airways Quick Reference Handbook (QRH) and the Airbus QRH ENG DUAL FAILURE procedures both provided guidance that indicated flaps 3 (conf3) was to be used for ditching.

F. REFERENCES

1. Bureau d'Enquetes et d'Analyses, *Technical Document: Preliminary video recording analysis, accident on January 15th 2009, at New York City, to the Airbus A320, registered N106US, operated by US Airways*, NTSB Accident Number DCA09MA026, Docket Item 98 (BEA n-us090115 vid01, May 15th, 2009). (Contact NTSB at pubinq@ntsb.gov).

2. National Transportation Safety Board, Office of Research and Engineering, *Flight Data Recorder Group Chairman's Factual Report, A320, Hudson River, New Jersey, January 15, 2009*, NTSB Accident Number DCA09MA026, Docket Item 84 (Washington, DC: NTSB, May 4, 2009). (Contact NTSB at pubinq@ntsb.gov).

3. National Transportation Safety Board, Office of Research and Engineering, *Cockpit Voice Recorder Group Chairman's Factual Report, Airbus Industrie A320-214, Weehawken, New Jersey, January 15, 2009*, NTSB Accident Number DCA09MA026, Docket Item 95 (Washington, DC: NTSB, April 22, 2009). (Contact NTSB at pubinq@ntsb.gov).

4. National Transportation Safety Board, Office of Research and Engineering, *Group Chairman's Aircraft Performance Study, American Airlines Flight 587, Airbus A300B4-605R, Belle Harbor, New York*, *November 12, 2001*, NTSB Accident Number DCA02MA001, Docket Item 188 (Washington, DC: NTSB, October 10, 2002). (Contact NTSB at pubinq@ntsb.gov).

5. Airbus Industrie, *US Airways 1549 NTSB Public Hearing: Fly-by-wire Protections, June 9-11, 2009*, presented by Terry Lutz, Experimental Test Pilot. (Available at http://www.ntsb.gov/events/2009/Weehawken-NJ/13-Lutz-presentation.pdf)

6. Airbus Industrie, *A320 Flight Crew Training Manual*.

7. National Transportation Safety Board, Office of Aviation Safety, *Simulator Evaluations for US Airways A320 Flight 1549 Accident, Ditching in Hudson River, 1/15/09 (NTSB # DCA09MA026),* Docket Item 35, (Washington, DC: NTSB, June 1, 2009). (Contact NTSB at pubinq@ntsb.gov).

8. Airbus Industrie, *A320 USA MSN 1044, Flight 1549 – Ditching simulation*, Airbus reference # D070ME0936142, dated 13 November 2009, Docket Item 116.

TABLES

EWR ASR Time HH:MM:SS EST	Range nmi	Azimuth ACPs	Mode C (MSL) Altitude feet	Latitude	Longitude	Distance East of LGA 4 nmi	Distance North of LGA 4 nmi
15:25:59.69	16.28	874	1000	N 40° 47' 33.27"	W 073° 51' 54.67"	0.86	1.40
15:26:04.16	16.38	867	1300	N 40° 47' 45.35"	W 073° 51' 53.76"	0.87	1.61
15:26:08.63	16.47	859	1600	N 40° 47' 58.56"	W 073° 51' 54.70"	0.86	1.83
15:26:13.37	16.52	850	1700	N 40° 48' 12.05"	W 073° 51' 59.58"	0.80	2.05
15:26:17.87	16.59	846	1900	N 40° 48' 19.39"	W 073° 51' 58.55"	0.81	2.17
15:26:22.61	16.64	839	1900	N 40° 48' 30.23"	W 073° 52' 01.87"	0.77	2.35
15:26:27.23	16.72	832	2000	N 40° 48' 41.94"	W 073° 52' 03.32"	0.75	2.55
15:26:31.73	16.78	825	2100	N 40° 48' 53.08"	W 073° 52' 06.33"	0.71	2.73
15:26:36.35	16.86	817	2200	N 40° 49' 06.18"	W 073° 52' 09.23"	0.68	2.95
15:26:41.09	16.94	809	2300	N 40° 49' 19.30"	W 073° 52' 12.38"	0.64	3.17
15:26:45.56	17.02	802	2400	N 40° 49' 31.11"	W 073° 52' 14.68"	0.61	3.37
15:26:50.18	17.11	793	2500	N 40° 49' 45.91"	W 073° 52' 18.77"	0.56	3.61
15:26:54.95	17.20	785	2600	N 40° 49' 59.42"	W 073° 52' 22.04"	0.52	3.84
15:26:59.57	17.30	777	2600	N 40° 50' 13.30"	W 073° 52' 24.88"	0.48	4.07
15:27:04.04	17.39	768	2700	N 40° 50' 28.17"	W 073° 52' 29.90"	0.42	4.32
15:27:08.78	17.50	761	2900	N 40° 50' 41.12"	W 073° 52' 31.51"	0.40	4.53
15:27:13.43	17.63	750	3000	N 40° 51' 00.05"	W 073° 52' 37.16"	0.32	4.85
15:27:17.90	17.73	742	3100	N 40° 51' 14.03"	W 073° 52' 41.27"	0.27	5.08
15:27:22.64	17.84	735	3200	N 40° 51' 27.12"	W 073° 52' 43.71"	0.24	5.30
15:27:27.11	17.95	727	3300	N 40° 51' 41.52"	W 073° 52' 47.75"	0.19	5.54
15:27:31.76	18.06	720	3300	N 40° 51' 54.68"	W 073° 52' 50.67"	0.15	5.76
15:27:36.23	18.16	714	3200	N 40° 52' 06.23"	W 073° 52' 52.99"	0.12	5.95
15:27:40.82	18.23	706	3000	N 40° 52' 19.20"	W 073° 53' 00.15"	0.03	6.17
15:27:45.59	18.27	697	2800	N 40° 52' 32.20"	W 073° 53' 10.82"	-0.10	6.38
15:27:50.21	18.23	690	2500	N 40° 52' 39.42"	W 073° 53' 23.44"	-0.26	6.50
15:27:54.83	18.16	681	2300	N 40° 52' 47.71"	W 073° 53' 40.91"	-0.48	6.64
15:27:59.30	18.00	675	2100	N 40° 52' 48.44"	W 073° 53' 59.10"	-0.71	6.65
15:28:03.92	17.78	671	1900	N 40° 52' 44.11"	W 073° 54' 17.64"	-0.95	6.58
15:28:08.51	17.53	666	1800	N 40° 52' 39.53"	W 073° 54' 39.28"	-1.22	6.51
15:28:13.28	17.27	665	1700	N 40° 52' 29.78"	W 073° 54' 55.45"	-1.42	6.34
15:28:17.75	17.00	664	1600	N 40° 52' 19.57"	W 073° 55' 12.15"	-1.64	6.17
15:28:22.37	16.73	666	1600	N 40° 52' 06.01"	W 073° 55' 24.55"	-1.79	5.95
15:28:26.99	16.47	667	1500	N 40° 51' 54.04"	W 073° 55' 37.86"	-1.96	5.75
15:28:31.61	16.22	670	1500	N 40° 51' 40.35"	W 073° 55' 47.92"	-2.09	5.52
15:28:36.20	15.97	671	1400	N 40° 51' 28.89"	W 073° 56' 00.80"	-2.25	5.33
15:28:40.85	15.70	673	1400	N 40° 51' 15.57"	W 073° 56' 13.56"	-2.41	5.11
15:28:45.59	15.45	675	1300	N 40° 51' 03.15"	W 073° 56' 25.25"	-2.56	4.90
15:28:50.06	15.20	675	1300	N 40° 50' 52.81"	W 073° 56' 39.59"	-2.74	4.73
15:28:54.68	14.95	678	1200	N 40° 50' 39.49"	W 073° 56' 50.17"	-2.88	4.51
15:28:59.27	14.72	678	1200	N 40° 50' 30.02"	W 073° 57' 03.42"	-3.04	4.35
15:29:04.04	14.47	680	1200	N 40° 50' 17.79"	W 073° 57' 15.41"	-3.20	4.15
15:29:08.66	14.23	682	1100	N 40° 50' 06.04"	W 073° 57' 26.90"	-3.34	3.95
15:29:13.13	14.02	682	1000	N 40° 49' 57.47"	W 073° 57' 39.04"	-3.49	3.81
15:29:17.75	13.77	684	900	N 40° 49' 45.40"	W 073° 57' 51.23"	-3.65	3.61
15:29:22.37	13.52	685	800	N 40° 49' 34.30"	W 073° 58' 04.62"	-3.82	3.42
15:29:26.99	13.28	686	700	N 40° 49' 23.65"	W 073° 58' 17.47"	-3.98	3.24
15:29:31.73	13.05	691	600	N 40° 49' 09.87"	W 073° 58' 25.52"	-4.08	3.01
15:29:36.35	12.81	695	500	N 40° 48' 56.70"	W 073° 58' 35.43"	-4.21	2.80
15:29:40.85	12.59	700	400	N 40° 48' 43.57"	W 073° 58' 43.32"	-4.31	2.58
15:29:45.44	12.36	702	300	N 40° 48' 32.74"	W 073° 58' 54.99"	-4.46	2.40
15:29:54.83	11.91	717	100	N 40° 48' 02.45"	W 073° 59' 07.68"	-4.62	1.89
15:30:13.31	11.14	737	300	N 40° 47' 16.87"	W 073° 59' 37.40"	-5.00	1.13
15:30:17.93	10.97	740	300	N 40° 47' 08.18"	W 073° 59' 45.52"	-5.10	0.99
15:30:22.52	10.81	745	300	N 40° 46' 58.35"	W 073° 59' 51.50"	-5.17	0.83
15:30:27.17	10.66	748	200	N 40° 46' 50.53"	W 073° 59' 58.56"	-5.26	0.70

Table 1a. EWR ASR-9 secondary returns for US1549 (beacon code 7134).

EWR ASR Time HH:MM:SS EST	Range nmi	Azimuth ACPs	Latitude	Longitude	Distance East of LGA 4, nmi	Distance North of LGA 4, nmi
15:26:36.35	17.84	755	N 40° 51' 01.32"	W 073° 52' 16.91"	0.58	4.87
15:26:45.56	17.78	756	N 40° 50' 57.86"	W 073° 52' 19.44"	0.55	4.81
15:26:50.18	17.75	754	N 40° 50' 59.43"	W 073° 52' 23.91"	0.49	4.84
15:26:54.95	17.75	756	N 40° 50' 56.80"	W 073° 52' 21.36"	0.52	4.79
15:26:59.57	17.69	753	N 40° 50' 58.59"	W 073° 52' 29.00"	0.43	4.82
15:27:04.04	17.66	757	N 40° 50' 52.28"	W 073° 52' 25.82"	0.47	4.72
15:27:08.78	17.56	758	N 40° 50' 47.43"	W 073° 52' 30.93"	0.40	4.64
15:27:09.26	17.56	758	N 40° 50' 47.43"	W 073° 52' 30.93"	0.40	4.64
15:27:22.64	17.53	756	N 40° 50' 48.97"	W 073° 52' 35.36"	0.35	4.66
15:27:22.64	17.53	756	N 40° 50' 48.97"	W 073° 52' 35.36"	0.35	4.66
15:27:27.11	17.72	760	N 40° 50' 50.46"	W 073° 52' 18.19"	0.56	4.69
15:27:27.71	17.72	760	N 40° 50' 50.46"	W 073° 52' 18.19"	0.56	4.69
15:27:41.12	17.69	765	N 40° 50' 42.79"	W 073° 52' 13.84"	0.62	4.56
15:27:41.72	17.69	765	N 40° 50' 42.79"	W 073° 52' 13.84"	0.62	4.56
15:27:45.59	17.66	763	N 40° 50' 44.39"	W 073° 52' 18.26"	0.56	4.59
15:27:46.16	17.66	763	N 40° 50' 44.39"	W 073° 52' 18.26"	0.56	4.59
15:27:54.95	17.59	771	N 40° 50' 31.37"	W 073° 52' 12.88"	0.63	4.37
15:27:54.95	17.59	771	N 40° 50' 31.37"	W 073° 52' 12.88"	0.63	4.37
15:27:59.45	17.56	762	N 40° 50' 42.19"	W 073° 52' 25.93"	0.47	4.55
15:28:00.17	17.56	762	N 40° 50' 42.19"	W 073° 52' 25.93"	0.47	4.55
15:28:22.49	17.47	774	N 40° 50' 23.27"	W 073° 52' 17.01"	0.58	4.24
15:28:27.11	17.47	777	N 40° 50' 19.30"	W 073° 52' 13.40"	0.63	4.17
15:28:31.73	17.44	771	N 40° 50' 26.20"	W 073° 52' 22.59"	0.51	4.28
15:28:36.50	17.41	776	N 40° 50' 18.58"	W 073° 52' 18.50"	0.56	4.16
15:28:45.74	17.34	771	N 40° 50' 22.75"	W 073° 52' 29.06"	0.43	4.23
15:28:54.80	17.41	771	N 40° 50' 25.16"	W 073° 52' 24.53"	0.48	4.27
15:28:59.57	17.44	774	N 40° 50' 22.25"	W 073° 52' 18.96"	0.56	4.22
15:29:08.81	17.50	774	N 40° 50' 24.30"	W 073° 52' 15.06"	0.60	4.25
15:29:50.21	17.41	766	N 40° 50' 31.71"	W 073° 52' 30.62"	0.41	4.38
15:30:04.07	17.31	767	N 40° 50' 26.93"	W 073° 52' 35.84"	0.34	4.30
15:30:08.66	17.28	766	N 40° 50' 27.18"	W 073° 52' 38.99"	0.30	4.30
15:30:22.52	17.22	765	N 40° 50' 26.38"	W 073° 52' 44.07"	0.24	4.29
15:30:27.17	17.19	769	N 40° 50' 20.17"	W 073° 52' 41.17"	0.27	4.18

Table 1b. Selected EWR ASR-9 primary returns near the flight path of US1549.

EWR ASR Time HH:MM:SS EST	CVR Transcript Text
15:24:54.00	[TWR] Cactus 1549 runway 4 clear for takeoff.
15:26:00.00	Cactus 1549 New York departure radar contact, climb and maintain 15000.
15:26:16.00	[HOT-2] and flaps one please.
15:26:52.00	[HOT-2] flaps up please, after takeoff checklist.
15:27:10.40	[HOT-1] birds.
15:27:11.40	[CAM] [sound of thump/thud(s) followed by shuddering sound]
15:27:15.00	[HOT-1] we got ... both of 'em rolling back.
15:27:21.30	[HOT-1] I'm starting the APU.
15:27:23.20	[HOT-1] my aircraft.
15:27:28.00	[HOT-1] get the QRH… loss of thrust on both engines.
15:27:32.90	[RDO-1] mayday mayday mayday... Cactus 1539 hit birds, we've lost thrust in both engines we're turning back towards LaGuardia.
15:27:42.00	[DEP] … you need to return to LaGuardia? Turn left heading of 220.
15:28:02.00	[HOT-2] airspeed optimum relight. 300 kts. we don't have that.
15:28:05.00	[DEP] Cactus 1529, ... do you want to try to land runway 13?
15:28:10.60	[RDO-1] we're unable. we may end up in the Hudson.
15:28:25.00	[HOT-1] ... the left one's coming back up a little bit.
15:28:31.00	[DEP] ... Cactus 1549 its gonna be left traffic for runway 31.
15:28:35.00	[RDO-1] unable.
15:28:36.00	[TCAS] traffic traffic. [DEP] OK, what do you need to land?
15:28:46.00	[DEP] Cactus 1529 runway 4's available if you wanna make left traffic to runway 4.
15:28:49.90	[RDO-1] I'm not sure we can make any runway. Uh what's over to our right anything in New Jersey maybe Teterboro?
15:28:55.00	[DEP] ok yeah, off your right side is Teterboro airport.
15:29:02.00	[DEP] you wanna try and go to Teterboro?
15:29:03.00	[RDO-1] yes.
15:29:11.00	[PA-1] this is the Captain brace for impact.
15:29:14.90	[GPWS] 1000.
15:29:21.00	[DEP] Cactus 1529 turn right 280, you can land runway one at Teterboro.
15:29:25.00	[RDO-1] we can't do it.
15:29:26.00	[HOT-1] go ahead, try number one.
15:29:27.00	[DEP] kay which runway would you like at Teterboro?
15:29:28.00	[RDO-1] we're gonna be in the Hudson.
15:29:44.00	[HOT-2] no relight.
15:29:45.40	[HOT-1] ok ...put the flaps out.
15:29:53.00	[DEP] Cactus 1549 radar contact is lost you also got Newark airport off your 2 o'clock in about 7 miles.
15:30:03.00	[HOT-2] 250 feet in the air.
15:30:11.00	[HOT-1] try the other one.
15:30:17.00	[HOT-2] got flaps two, you want more?
15:30:19.00	[HOT-1] no let’s stay at two.
15:30:38.00	[HOT-1] we're gonna brace.
15:30:41.10	[GPWS] 50.
15:30:43.70	[End of Recording]

Table 2. Selected CVR events. For complete list of CVR events, see Reference 3.

Segment #	Start time	End time	Speed bias, knots	Track bias, degrees	Rate of climb bias, ft/min	n_x bias, G's	n_y bias, G's	nlf bias, G's	Groundspeed/drift correction vector magnitude, knots	Groundspeed/drift correction vector direction, degrees
1	15:25:07	15:25:47	0	0	0	0.00473	0.00343	-0.00726	0	0
2	15:25:47	15:27:17	0	0	0	0.00532	0.00579	-0.00823	2.7	259.5
3	15:27:17	15:28:47	0	0	0	0.00399	0.00570	-0.00703	5.3	145.7
4	15:28:47	15:29:47	0.6	-0.2	79.7	0.00307	0.00365	-0.00890	0	0
5	15:29:47	15:30:44	0	0	0	0.00390	0.01283	-0.00754	6.9	146.8

Table 3. Accelerometer integration segments.

FIGURES

Figure 1. Touchdown location based on BEA analysis of video footage of the water landing. “Toucher queue” is the touchdown point, and “immobilization” is the point where the airplane came to rest relative to the water.

DCA09MA026: US Airways flight 1549, Airbus A320-214, Weehawken, NJ, January 15, 2009

Plan view of flight path based on radar and FDR data

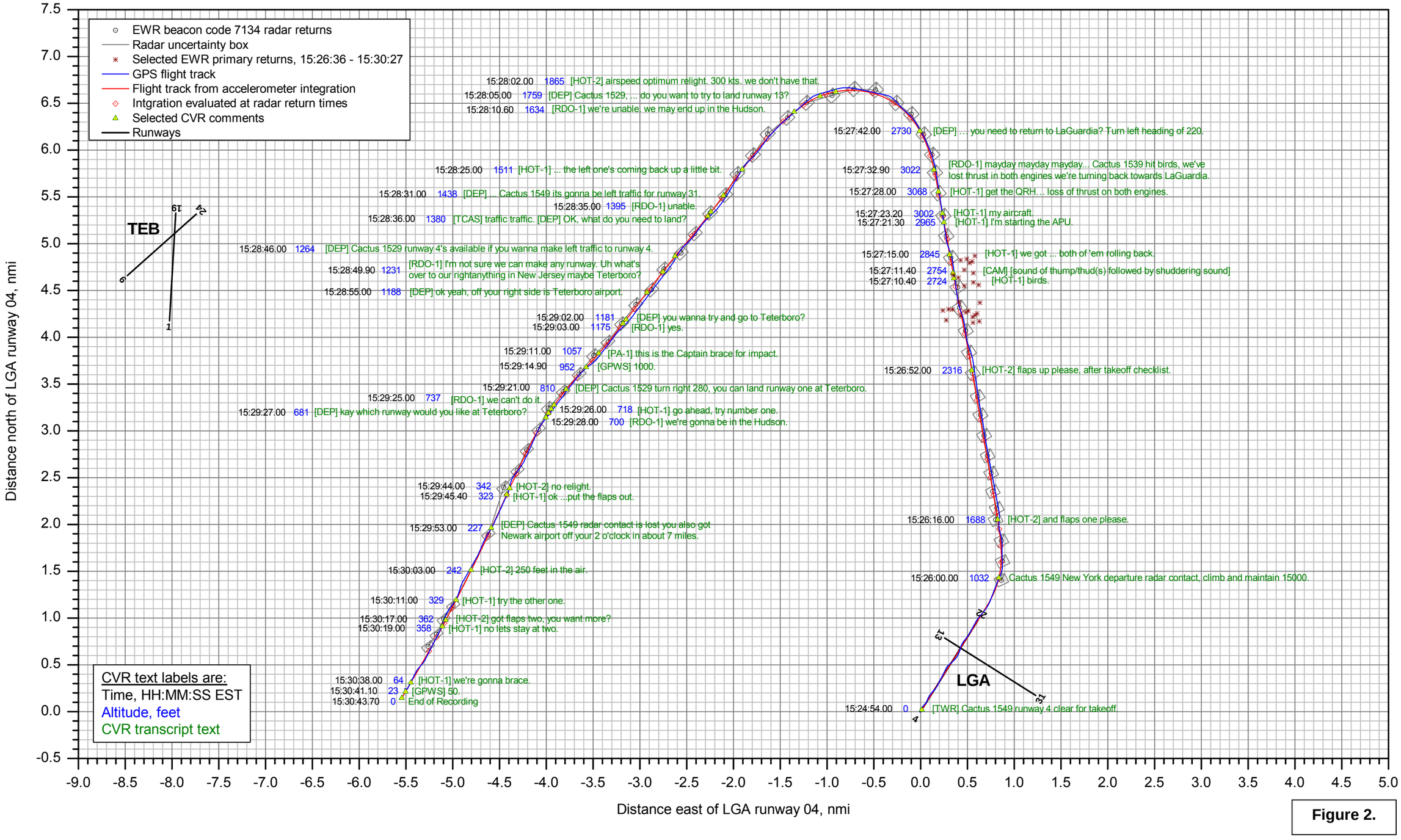

Figure 2.

DCA09MA026: US Airways flight 1549, Airbus A320-214, Weehawken, NJ, January 15, 2009

Plan view of flight path based on radar and FDR data

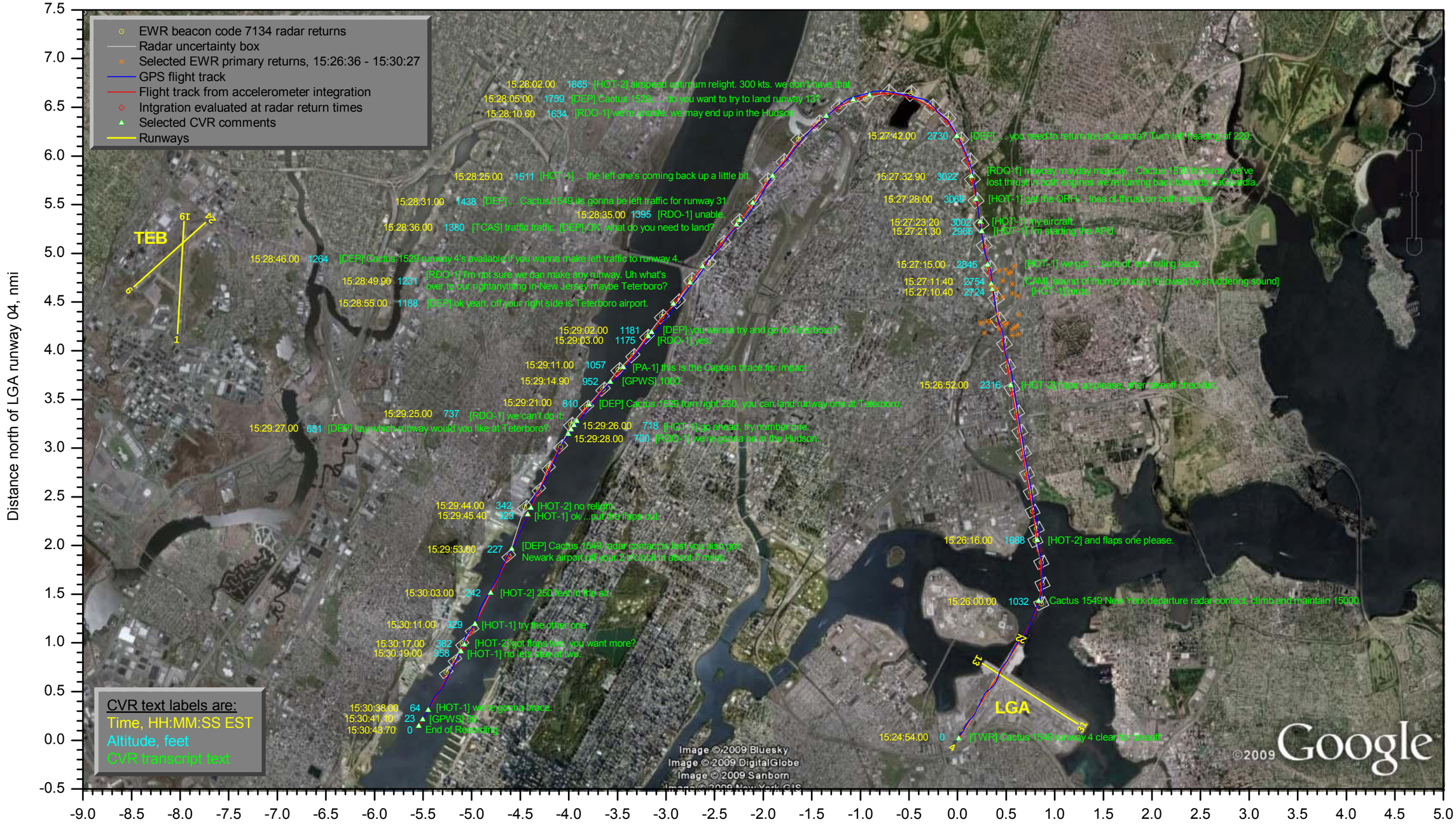

Figure 3.

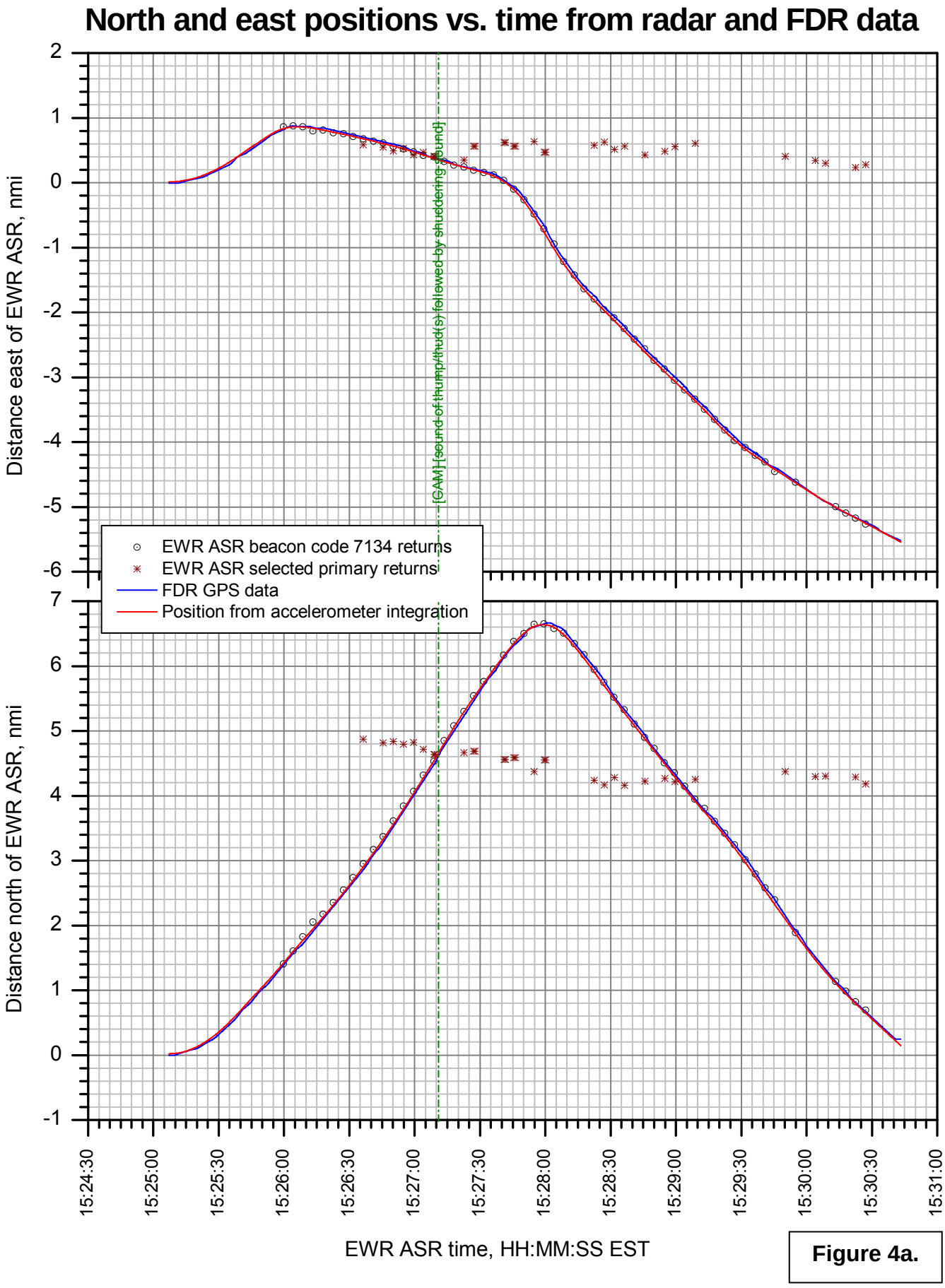
North and east positions vs. time from radar and FDR data
Distance east of EWR ASR, nmi
Distance north of EWR ASR, nmi
EWR ASR time, HH:MM:SS EST
EWR ASR beacon code 7134 returns
EWR ASR selected primary returns
FDR GPS data
Position from accelerometer integration
[CAM] [sound of thump/thud(s) followed by shuddering sound]
2
1
0
-1
-2
-3
-4
-5
-6
7
6
5
4
3
2
1
0
-1
15:24:30
15:25:00
15:25:30
15:26:00
15:26:30
15:27:00
15:27:30
15:28:00
15:28:30
15:29:00
15:29:30
15:30:00
15:30:30
15:31:00

Figure 4a.

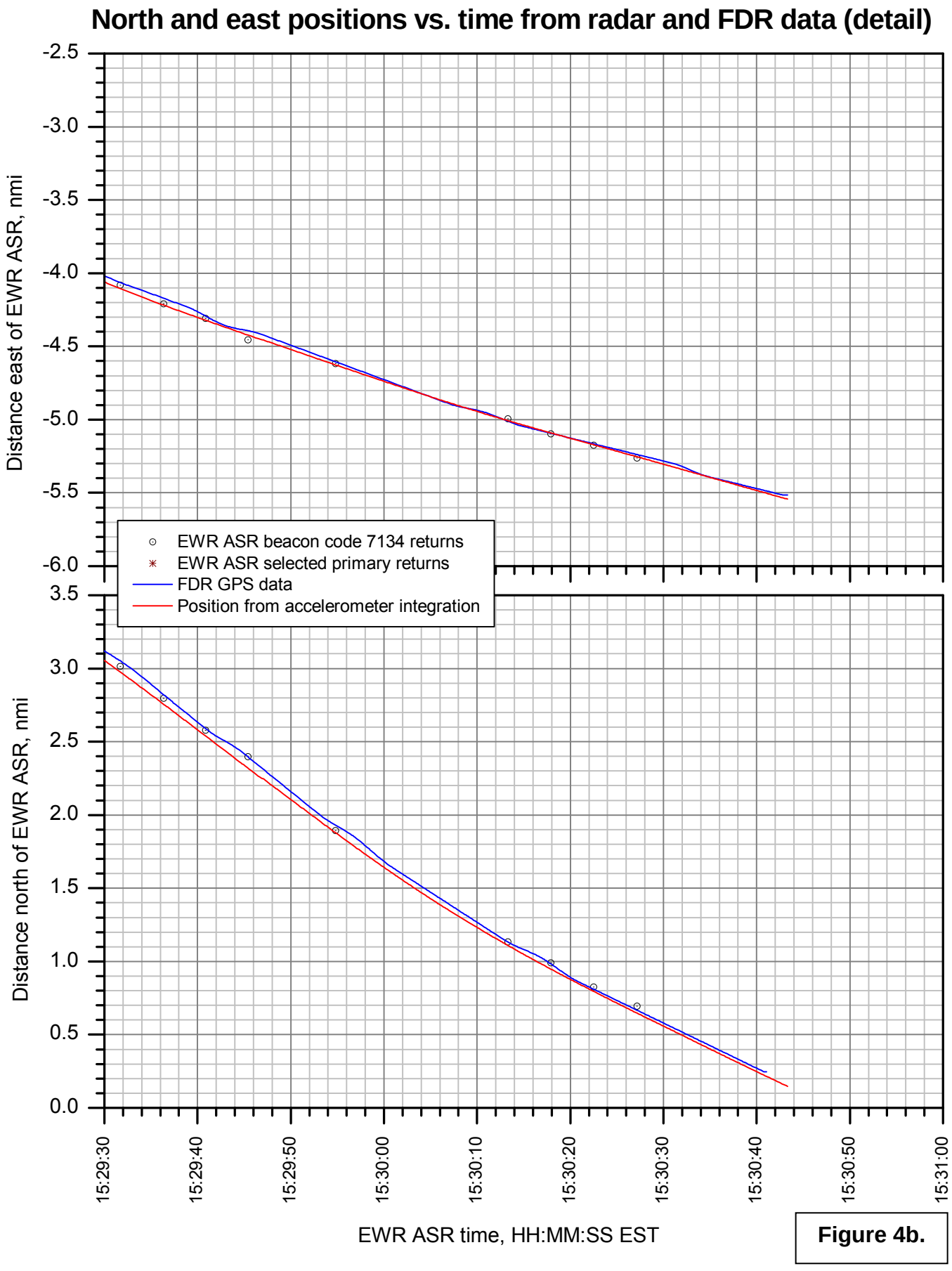
North and east positions vs. time from radar and FDR data (detail)
Distance east of EWR ASR, nmi
-2.5
-3.0
-3.5
-4.0
-4.5
-5.0
-5.5
-6.0
EWR ASR beacon code 7134 returns
EWR ASR selected primary returns
FDR GPS data
Position from accelerometer integration
Distance north of EWR ASR, nmi
3.5
3.0
2.5
2.0
1.5
1.0
0.5
0.0
15:29:30
15:29:40
15:29:50
15:30:00
15:30:10
15:30:20
15:30:30
15:30:40
15:30:50
15:31:00
EWR ASR time, HH:MM:SS EST

Figure 4b.

DCA09MA026: US Airways flight 1549, Airbus A320-214, Weehawken, NJ, January 15, 2009

Recorded and computed altitude data

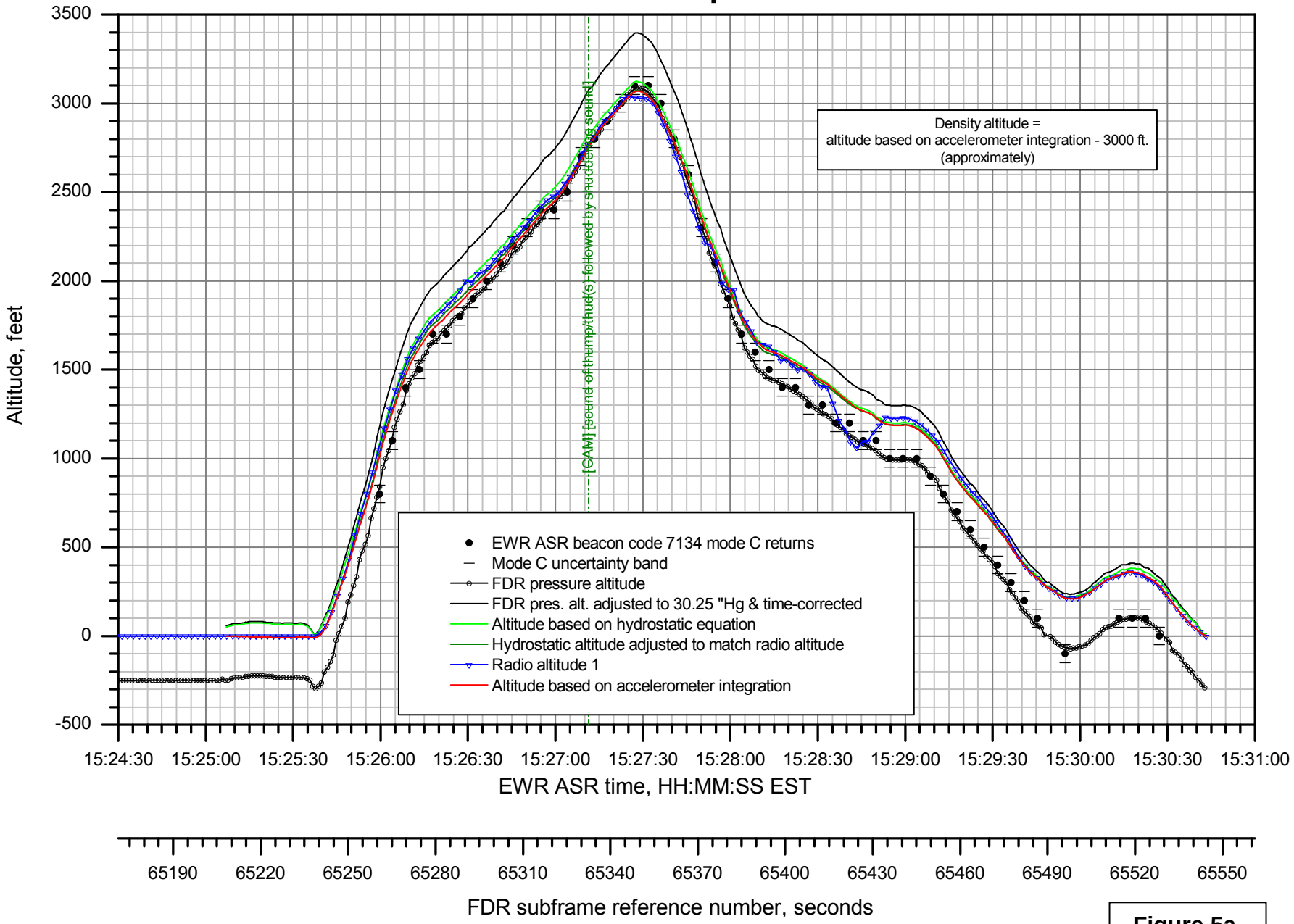

Figure 5a.

DCA09MA026: US Airways flight 1549, Airbus A320-214, Weehawken, NJ, January 15, 2009

Recorded and computed altitude data (detail)

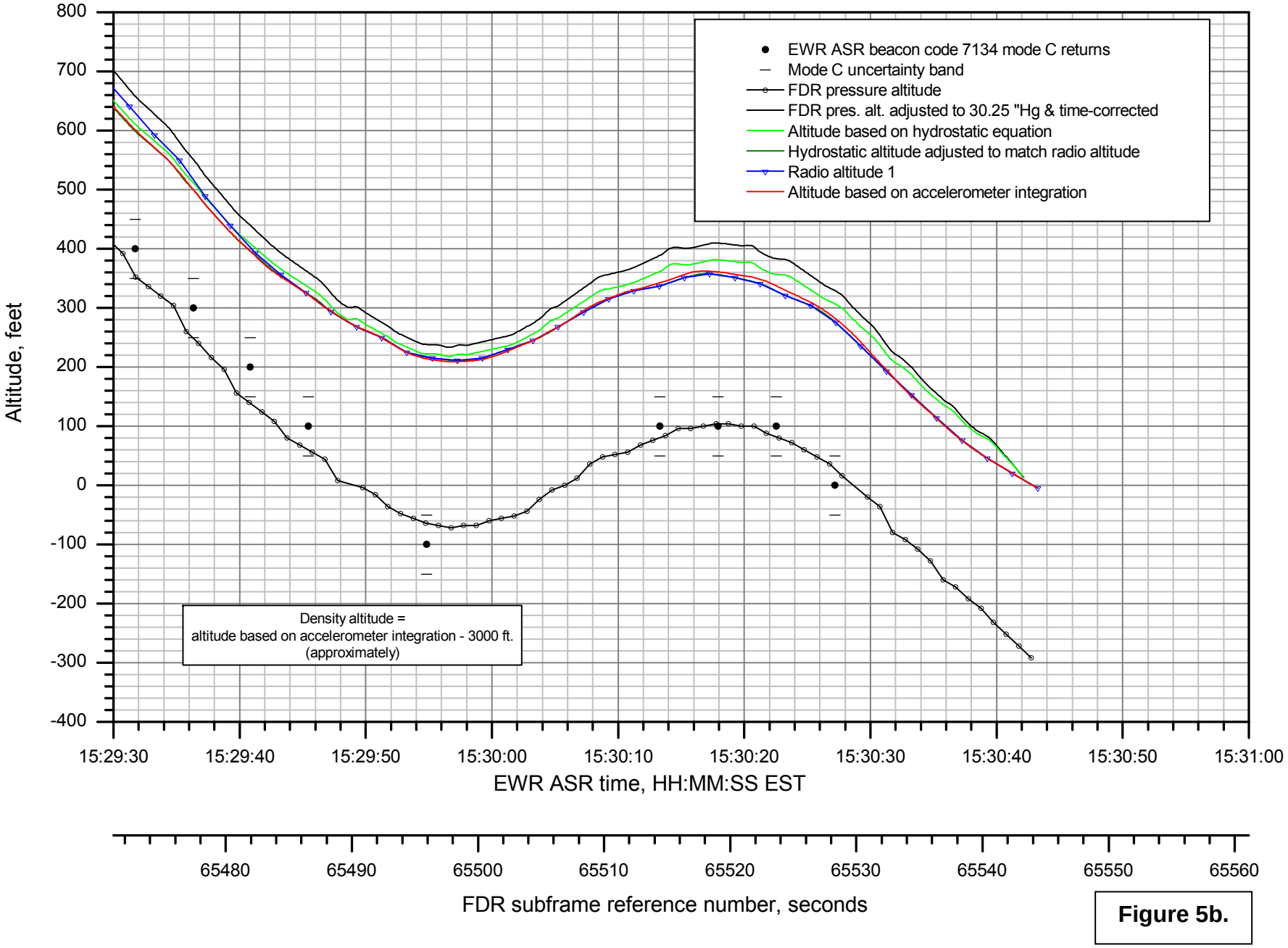

Figure 5b.

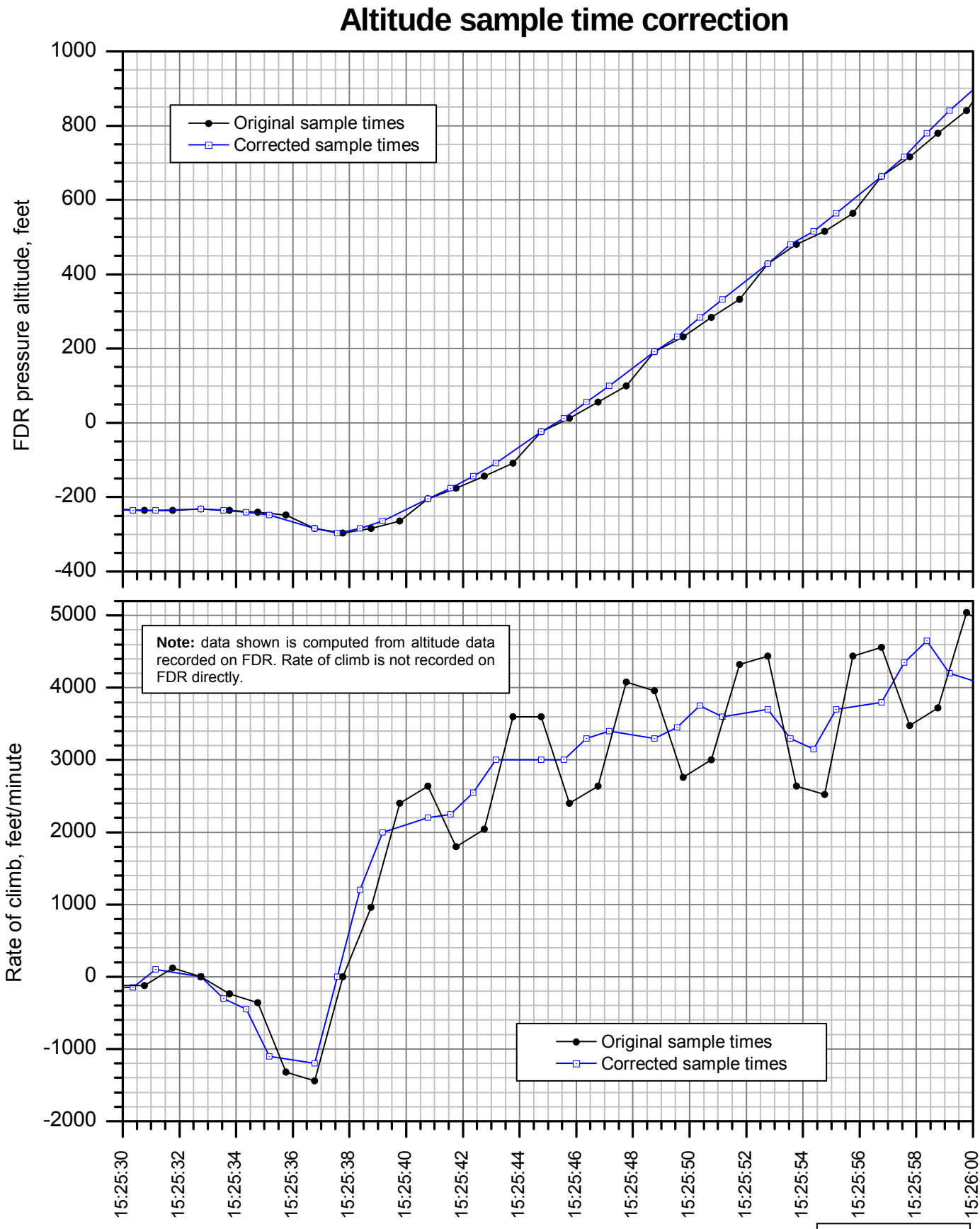
Altitude sample time correction
FDR pressure altitude, feet
1000
800
600
400
200
0
-200
-400
Original sample times
Corrected sample times
Rate of climb, feet/minute
5000
4000
3000
2000
1000
0
-1000
-2000
Note: data shown is computed from altitude data recorded on FDR. Rate of climb is not recorded on FDR directly.
Original sample times
Corrected sample times
15:25:30
15:25:32
15:25:34
15:25:36
15:25:38
15:25:40
15:25:42
15:25:44
15:25:46
15:25:48
15:25:50
15:25:52
15:25:54
15:25:56
15:25:58
15:26:00
EWR ASR time, HH:MM:SS EST

Figure 5c.

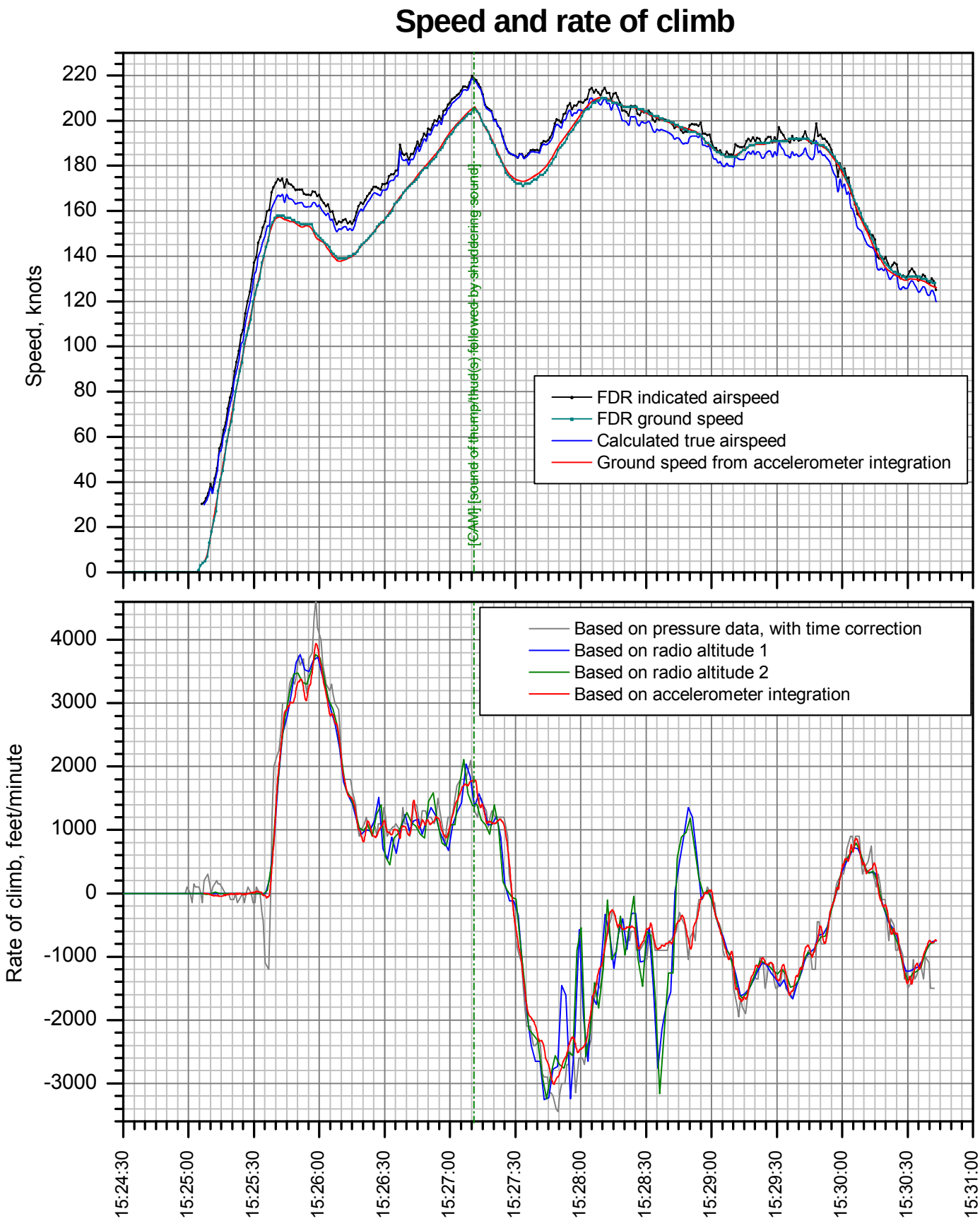
Speed and rate of climb
Speed, knots
220
200
180
160
140
120
100
80
60
40
20
0
[CAM] [sound of thump/thud(s) followed by shuddering sound]
FDR indicated airspeed
FDR ground speed
Calculated true airspeed
Ground speed from accelerometer integration
Rate of climb, feet/minute
4000
3000
2000
1000
0
-1000
-2000
-3000
Based on pressure data, with time correction
Based on radio altitude 1
Based on radio altitude 2
Based on accelerometer integration
15:24:30
15:25:00
15:25:30
15:26:00
15:26:30
15:27:00
15:27:30
15:28:00
15:28:30
15:29:00
15:29:30
15:30:00
15:30:30
15:31:00
EWR ASR time, HH:MM:SS EST

Figure 6a.

DCA09MA026: US Airways flight 1549, Airbus A320-214, Weehawken, NJ, January 15, 2009

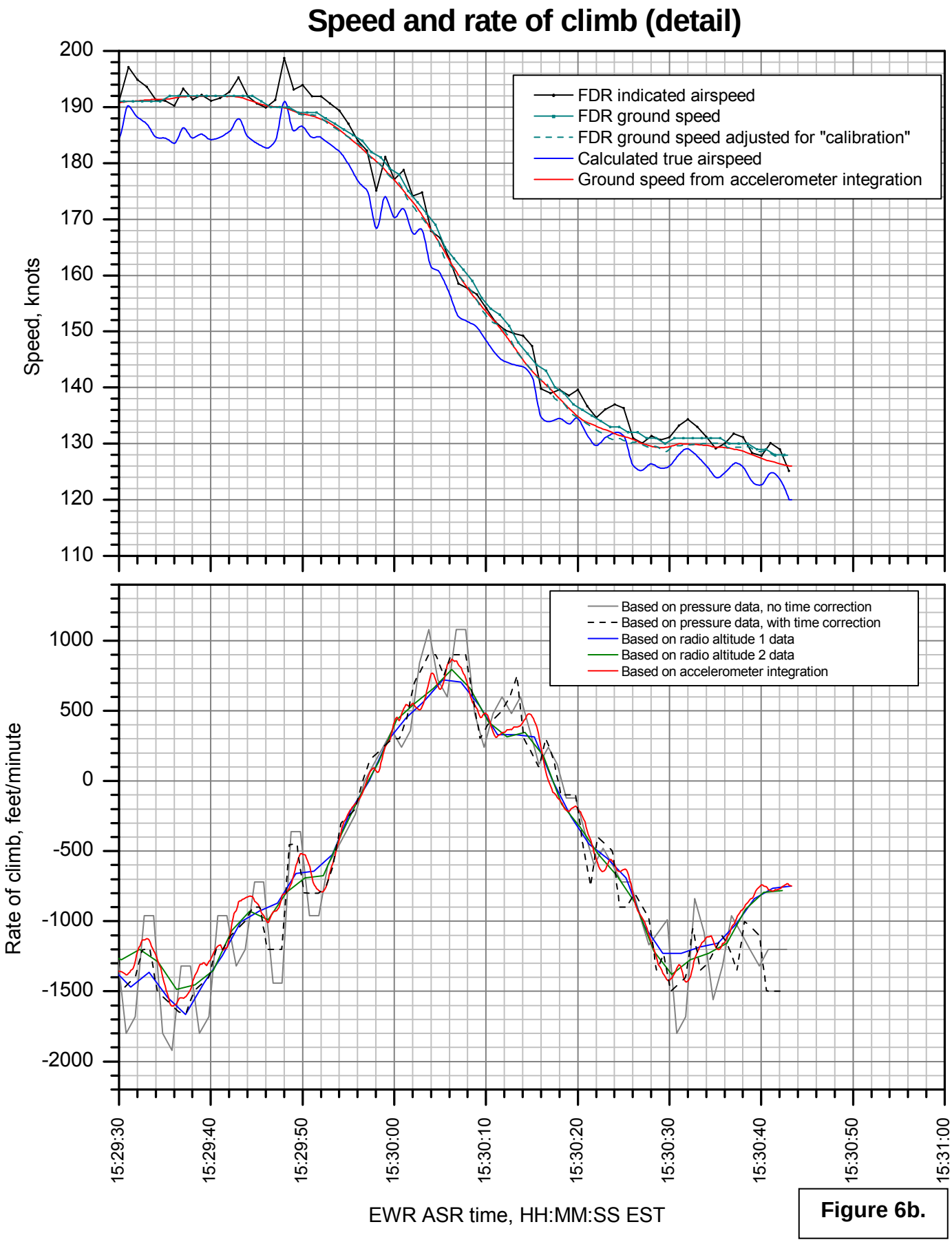

Figure 6b.

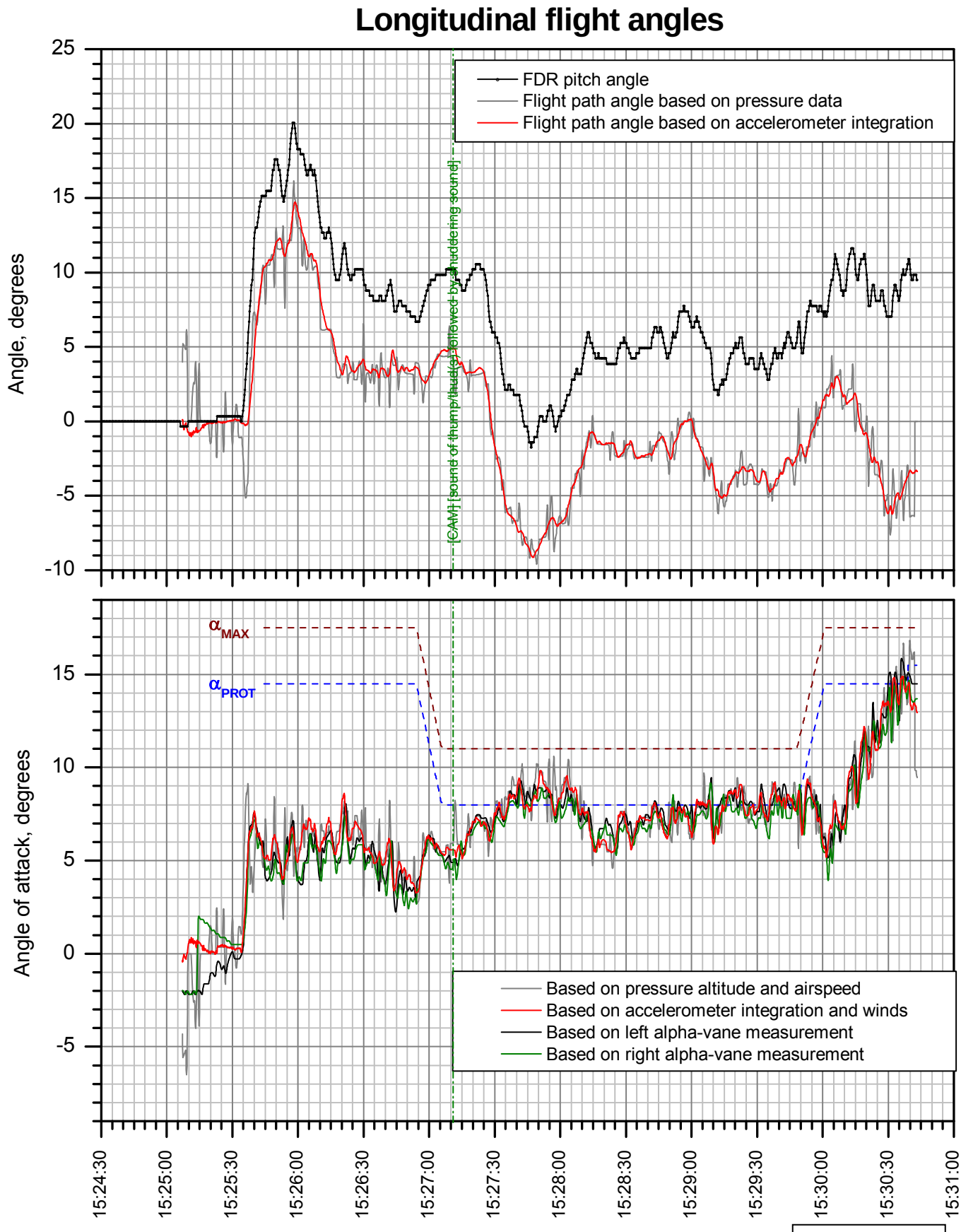
Longitudinal flight angles
FDR pitch angle
Flight path angle based on pressure data
Flight path angle based on accelerometer integration
[CAM] [sound of thump/thud(?) followed by a shuddering sound]
Angle, degrees
25
20
15
10
5
0
-5
-10
α_{MAX}
α_{PROT}
Based on pressure altitude and airspeed
Based on accelerometer integration and winds
Based on left alpha-vane measurement
Based on right alpha-vane measurement
Angle of attack, degrees
15
10
5
0
-5
15:24:30
15:25:00
15:25:30
15:26:00
15:26:30
15:27:00
15:27:30
15:28:00
15:28:30
15:29:00
15:29:30
15:30:00
15:30:30
15:31:00
EWR ASR time, HH:MM:SS EST

Figure 7a.

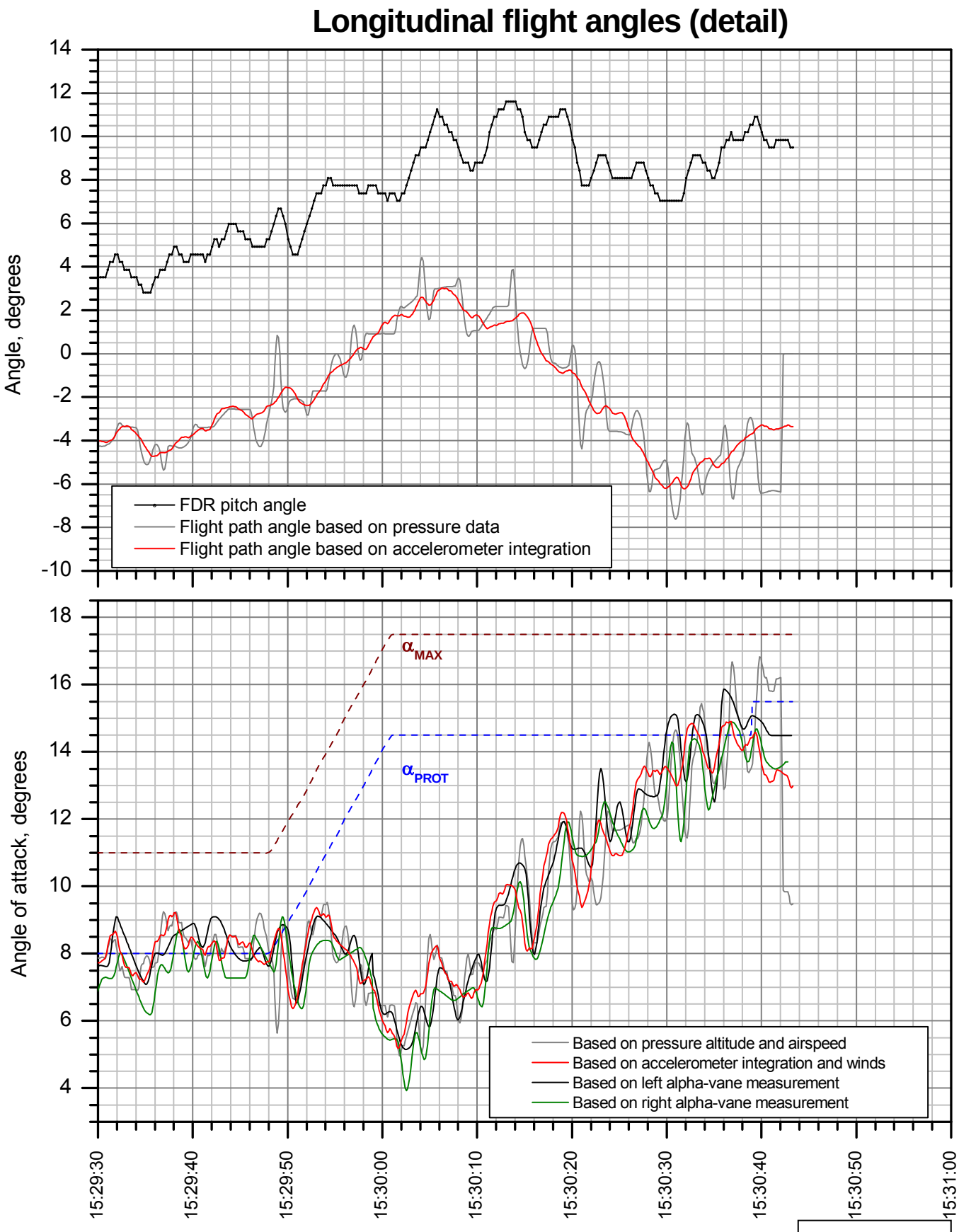
Longitudinal flight angles (detail)
Angle, degrees
14
12
10
8
6
4
2
0
-2
-4
-6
-8
-10
FDR pitch angle
Flight path angle based on pressure data
Flight path angle based on accelerometer integration
Angle of attack, degrees
18
16
14
12
10
8
6
4
α_{MAX}
α_{PROT}
Based on pressure altitude and airspeed
Based on accelerometer integration and winds
Based on left alpha-vane measurement
Based on right alpha-vane measurement
15:29:30
15:29:40
15:29:50
15:30:00
15:30:10
15:30:20
15:30:30
15:30:40
15:30:50
15:31:00
EWR ASR time, HH:MM:SS EST

Figure 7b.

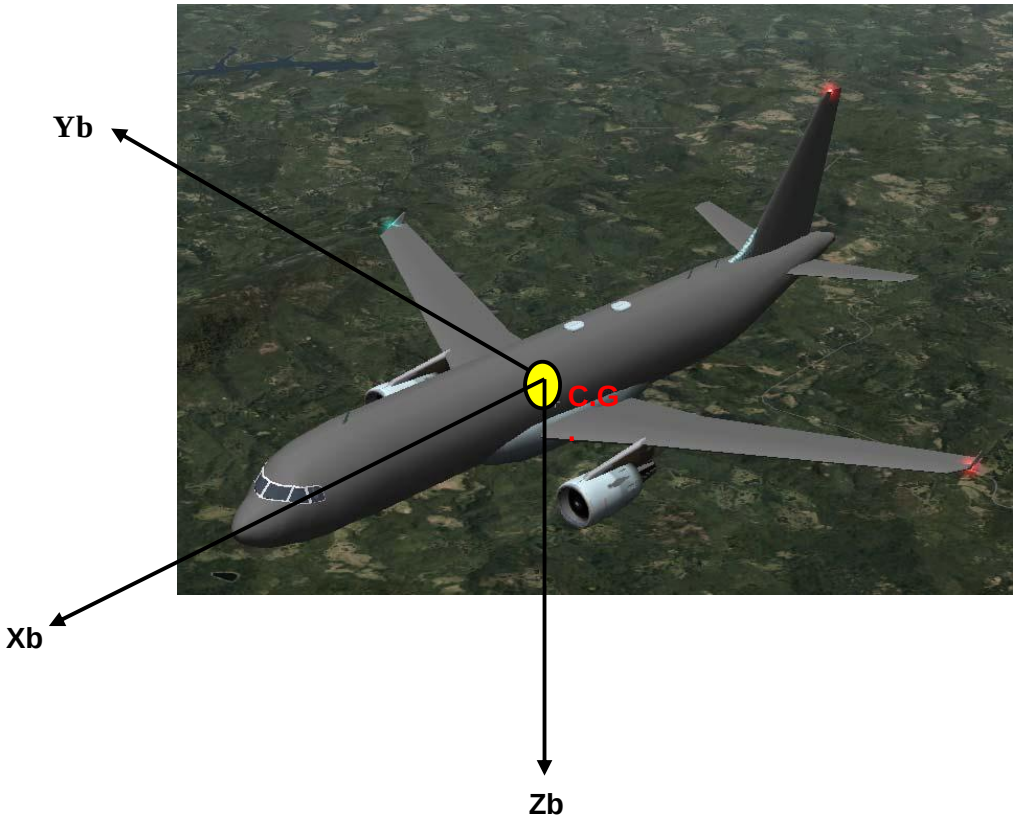

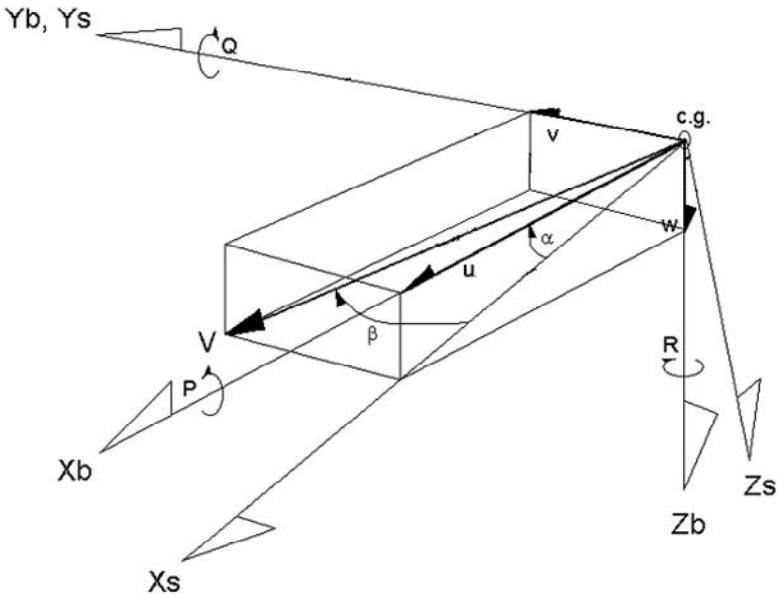

C.G. = center of gravity

{Xb, Yb, Zb} = body axis system

{Xs, Ys, Zs} = stability axis system

V = velocity vector

α = angle of attack

β = sideslip angle

P = body axis roll rate

Q = body axis pitch rate

R = body axis yaw rate

u = component of V along Xb

v = component of V along Yb

w = component of V along Zb

Figure 8.

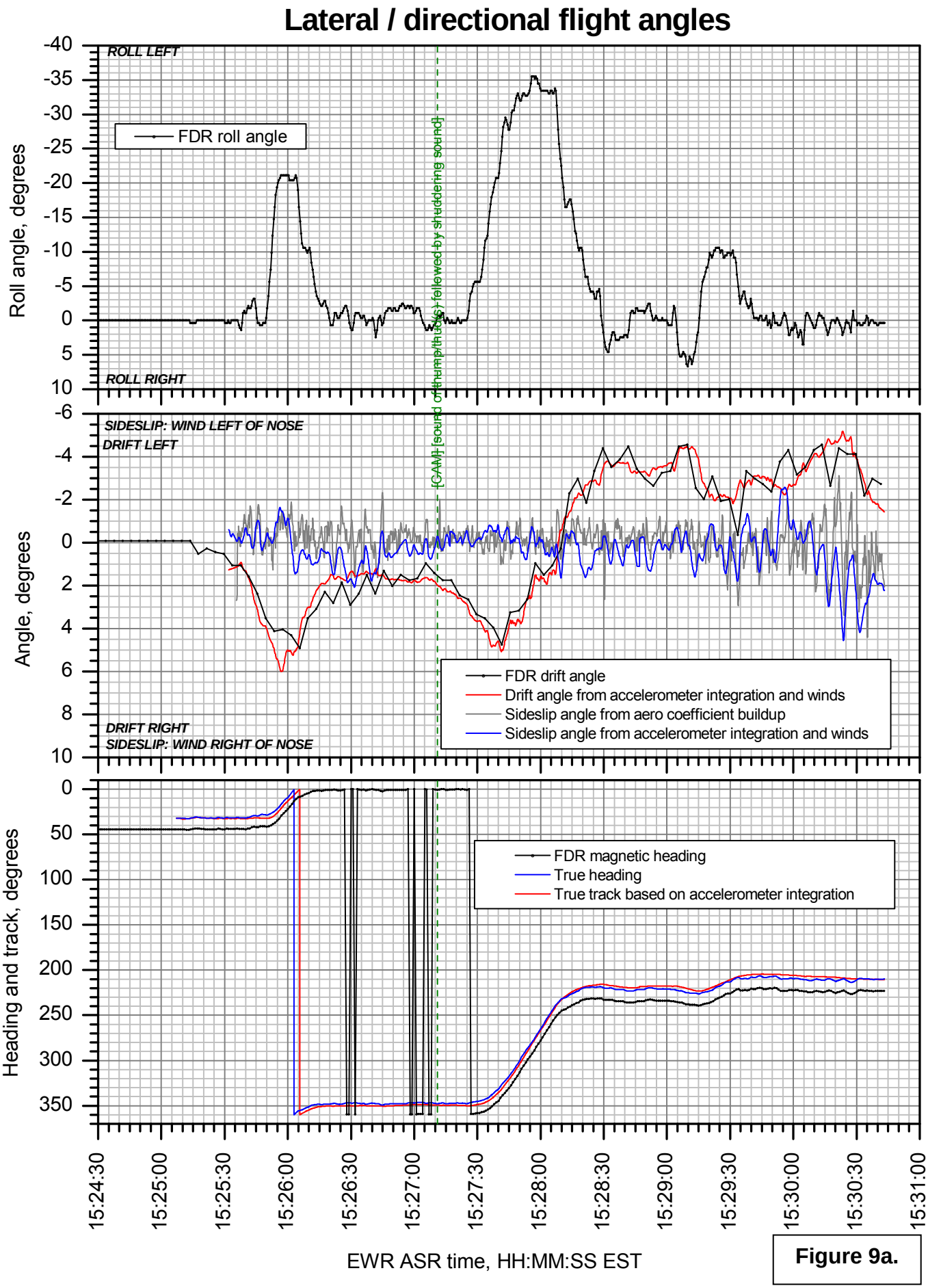
Lateral / directional flight angles
ROLL LEFT
ROLL RIGHT
FDR roll angle
Roll angle, degrees
-40
-35
-30
-25
-20
-15
-10
-5
0
5
10
[CAM] [sound of thump/thud] followed by shuddering sound
SIDESLIP: WIND LEFT OF NOSE
DRIFT LEFT
DRIFT RIGHT
SIDESLIP: WIND RIGHT OF NOSE
Angle, degrees
-6
-4
-2
0
2
4
6
8
10
FDR drift angle
Drift angle from accelerometer integration and winds
Sideslip angle from aero coefficient buildup
Sideslip angle from accelerometer integration and winds
Heading and track, degrees
0
50
100
150
200
250
300
350
FDR magnetic heading
True heading
True track based on accelerometer integration
15:24:30
15:25:00
15:25:30
15:26:00
15:26:30
15:27:00
15:27:30
15:28:00
15:28:30
15:29:00
15:29:30
15:30:00
15:30:30
15:31:00
EWR ASR time, HH:MM:SS EST

Figure 9a.

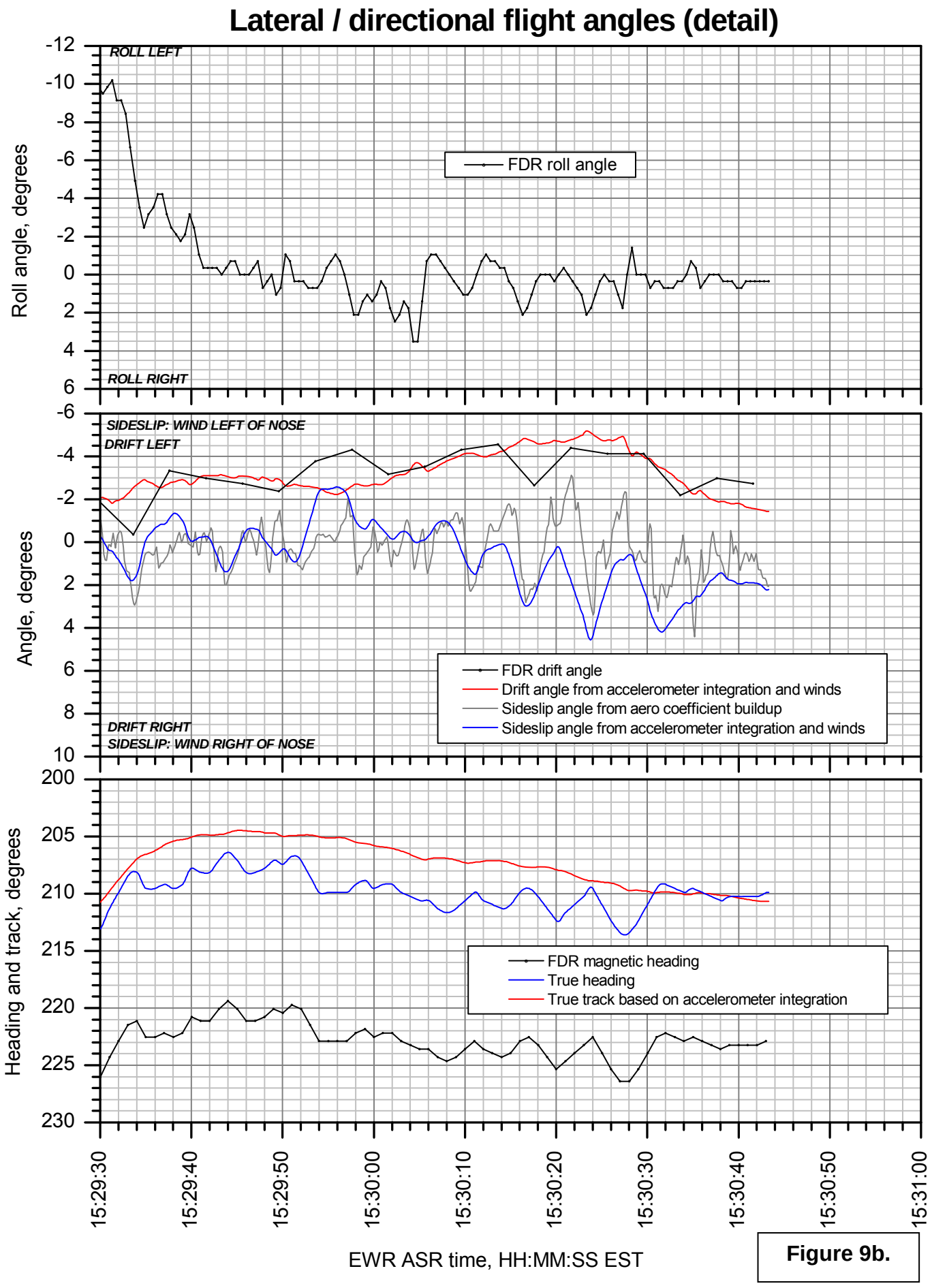
Lateral / directional flight angles (detail)
ROLL LEFT
ROLL RIGHT
Roll angle, degrees
FDR roll angle
SIDESLIP: WIND LEFT OF NOSE
DRIFT LEFT
DRIFT RIGHT
SIDESLIP: WIND RIGHT OF NOSE
Angle, degrees
FDR drift angle
Drift angle from accelerometer integration and winds
Sideslip angle from aero coefficient buildup
Sideslip angle from accelerometer integration and winds
Heading and track, degrees
FDR magnetic heading
True heading
True track based on accelerometer integration
15:29:30
15:29:40
15:29:50
15:30:00
15:30:10
15:30:20
15:30:30
15:30:40
15:30:50
15:31:00
EWR ASR time, HH:MM:SS EST

Figure 9b.

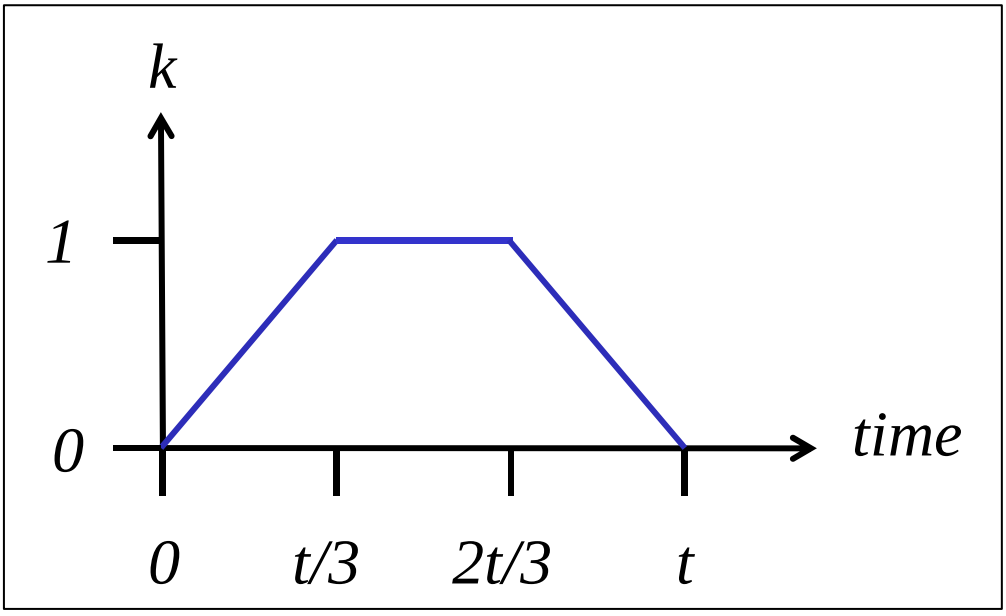

Figure 10. k – factor for velocity vector addition to velocity defined by FDR groundspeed and drift angle.

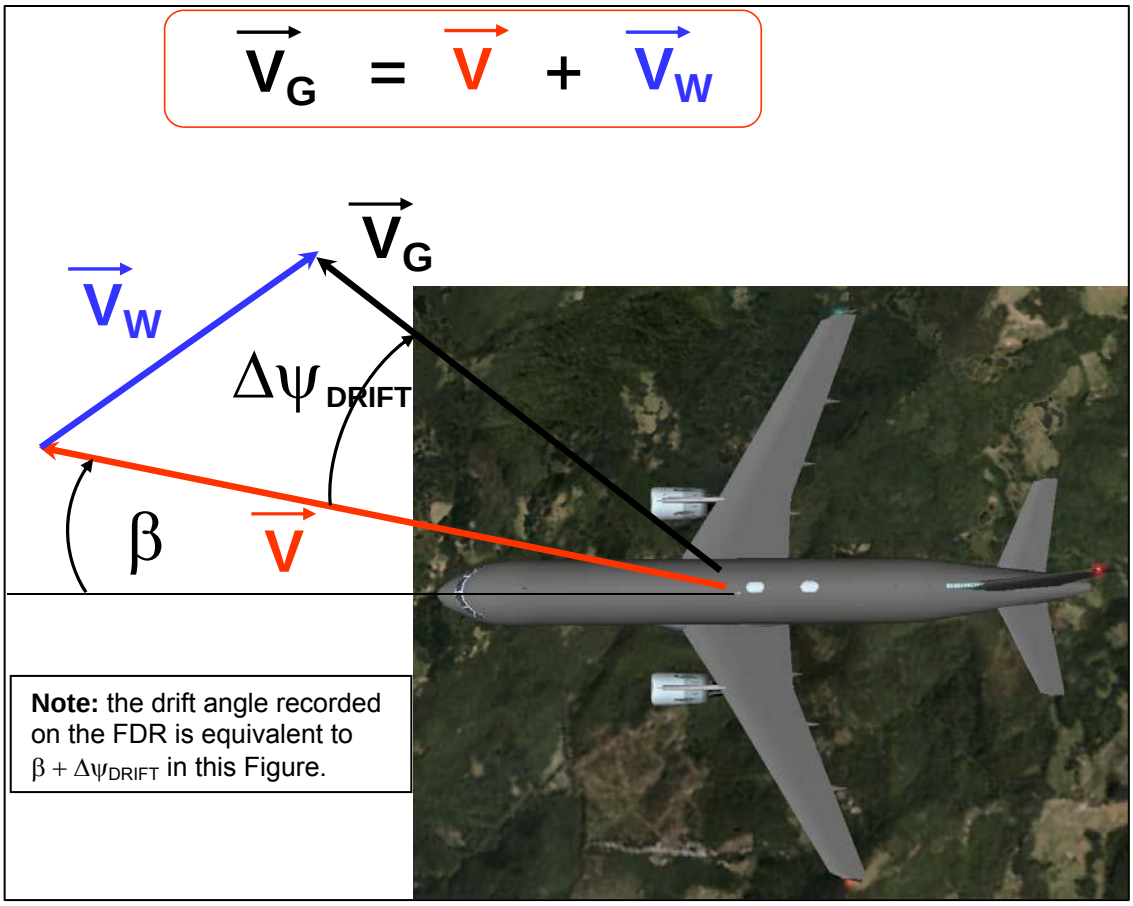

Figure 11. Wind triangle.

DCA09MA026: US Airways flight 1549, Airbus A320-214, Weehawken, NJ, January 15, 2009

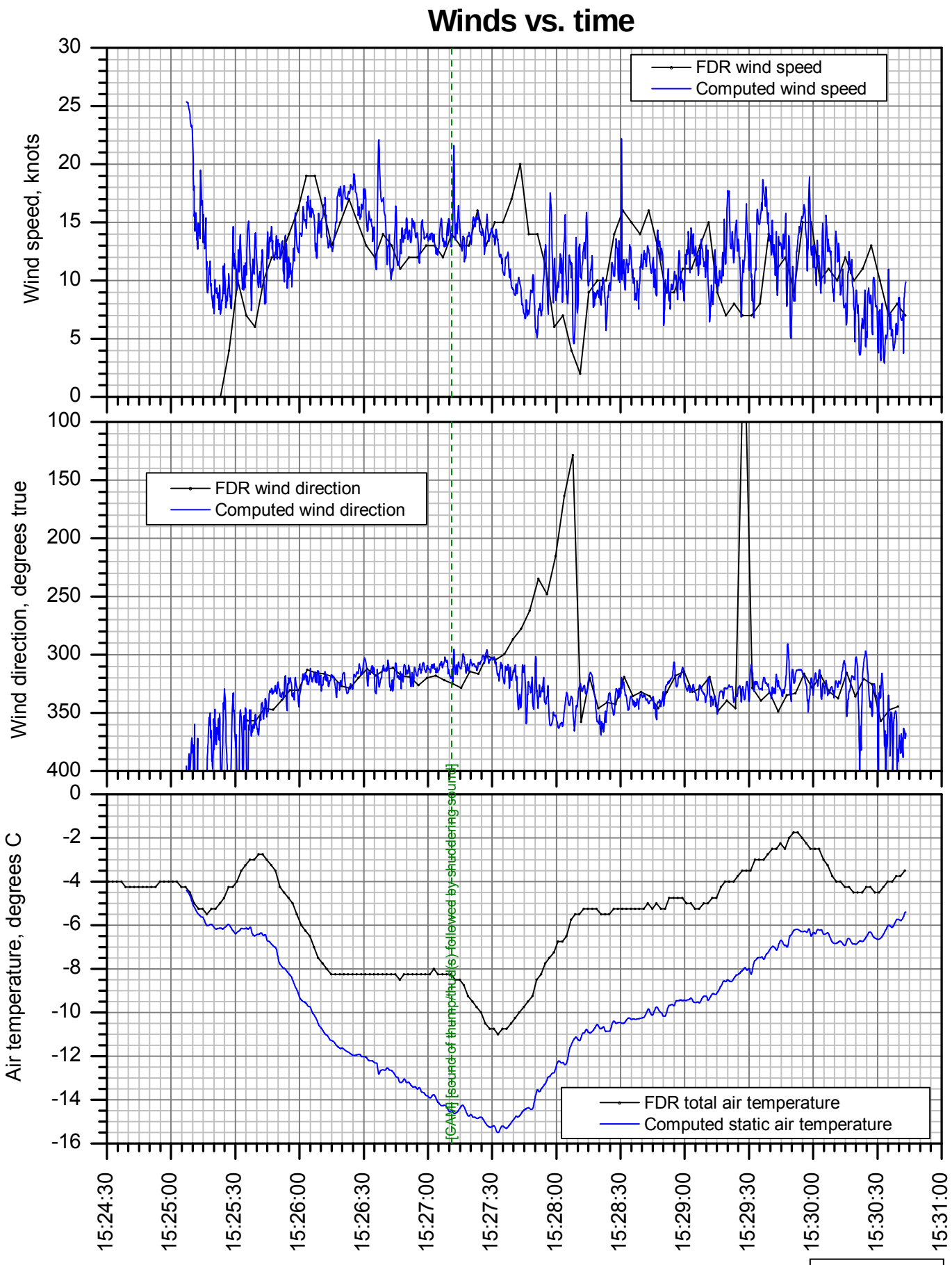

Figure 12

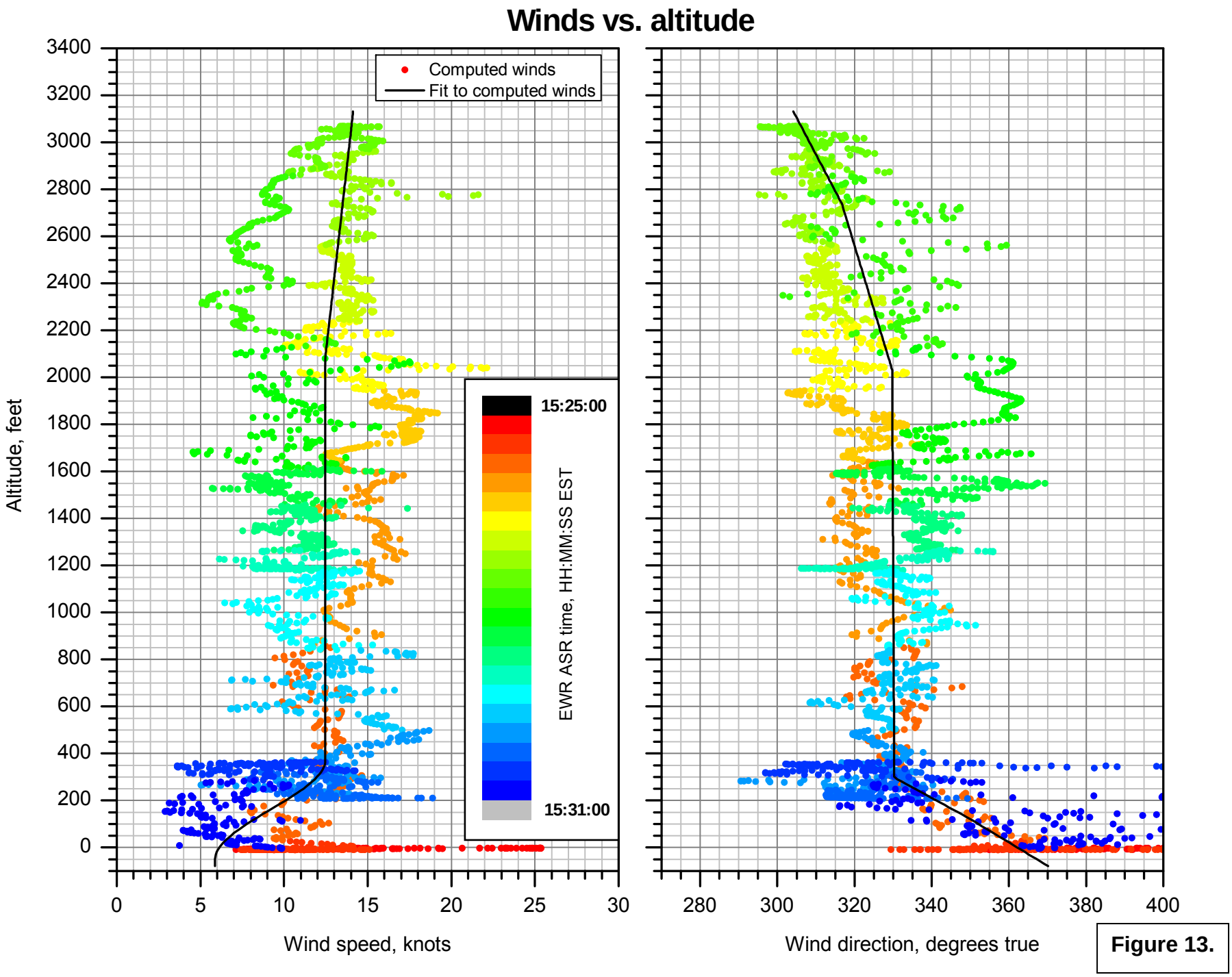
Winds vs. altitude
Computed winds
Fit to computed winds
Altitude, feet
3400
3200
3000
2800
2600
2400
2200
2000
1800
1600
1400
1200
1000
800
600
400
200
0
15:25:00
EWR ASR time, HH:MM:SS EST
15:31:00
0
5
10
15
20
25
30
Wind speed, knots
280
300
320
340
360
380
400
Wind direction, degrees true

Figure 13.

Flight controls

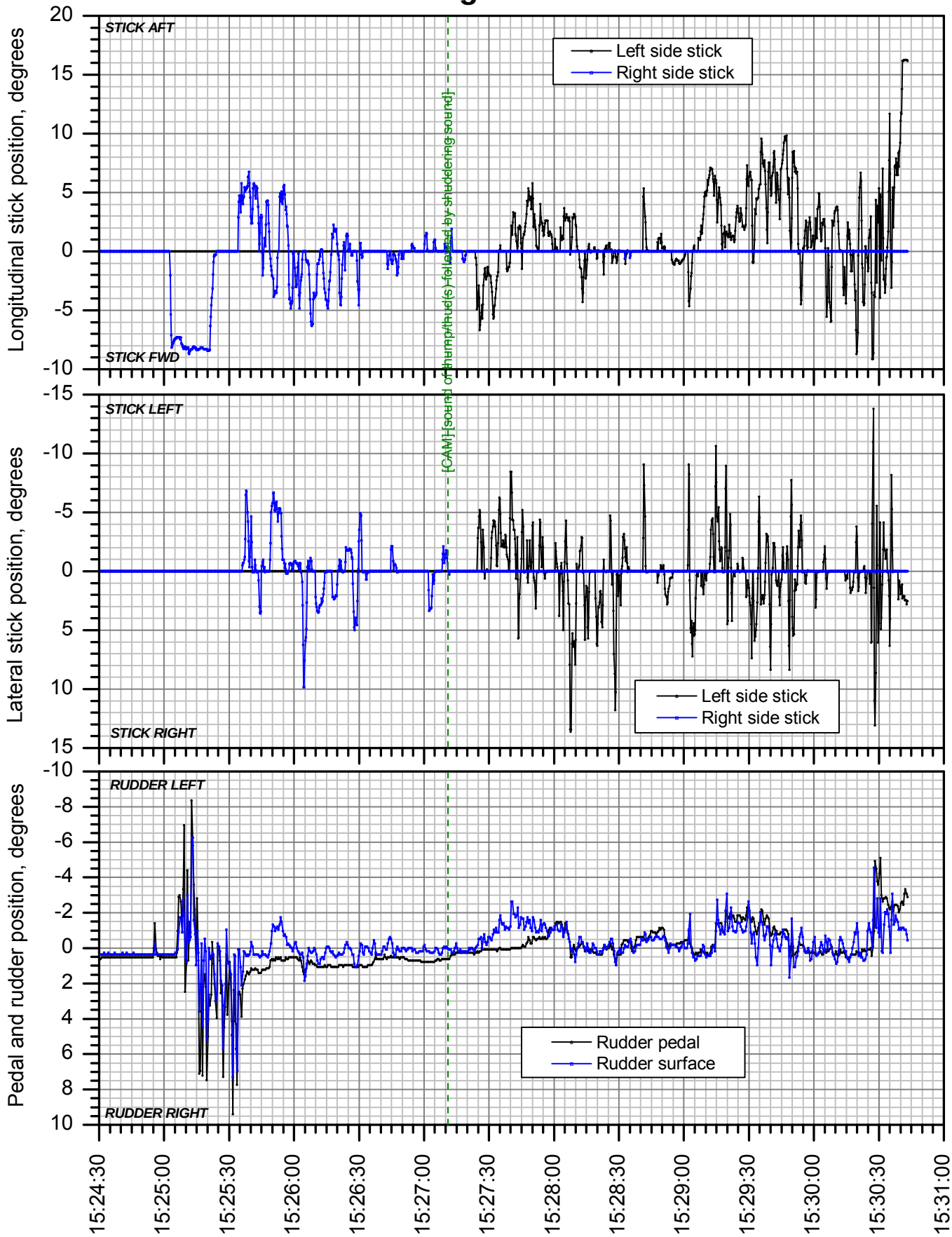

Figure 14a.

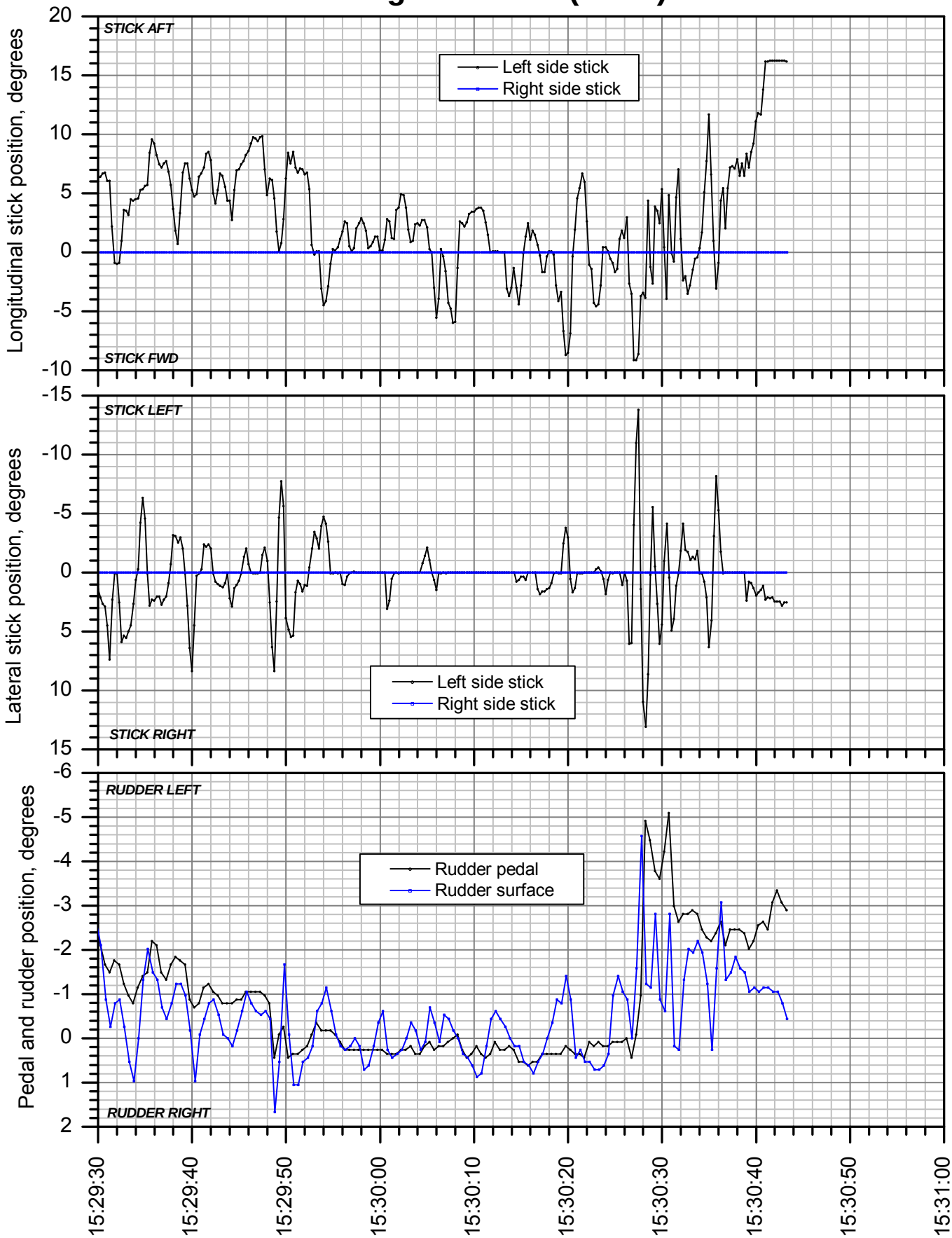
Flight controls (detail)
Longitudinal stick position, degrees
STICK AFT
STICK FWD
Left side stick
Right side stick
Lateral stick position, degrees
STICK LEFT
STICK RIGHT
Left side stick
Right side stick
Pedal and rudder position, degrees
RUDDER LEFT
RUDDER RIGHT
Rudder pedal
Rudder surface
15:29:30
15:29:40
15:29:50
15:30:00
15:30:10
15:30:20
15:30:30
15:30:40
15:30:50
15:31:00
EWR ASR time, HH:MM:SS EST

Figure 14b.

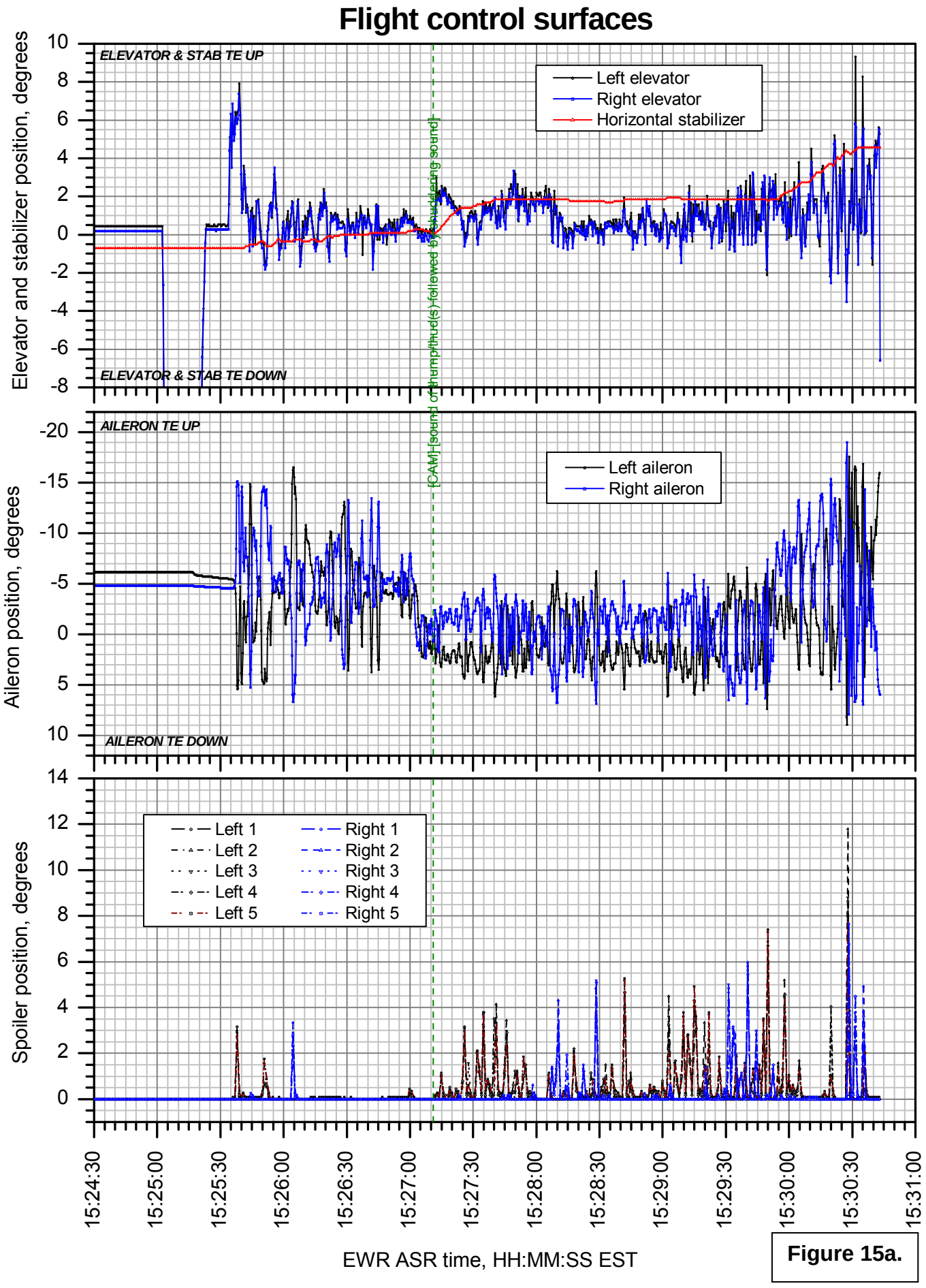
Flight control surfaces
Elevator and stabilizer position, degrees
ELEVATOR & STAB TE UP
ELEVATOR & STAB TE DOWN
Left elevator
Right elevator
Horizontal stabilizer
[CAM] [sound of thump/thud(s) followed by clattering sound]
Aileron position, degrees
AILERON TE UP
AILERON TE DOWN
Left aileron
Right aileron
Spoiler position, degrees
Left 1
Left 2
Left 3
Left 4
Left 5
Right 1
Right 2
Right 3
Right 4
Right 5
15:24:30
15:25:00
15:25:30
15:26:00
15:26:30
15:27:00
15:27:30
15:28:00
15:28:30
15:29:00
15:29:30
15:30:00
15:30:30
15:31:00
EWR ASR time, HH:MM:SS EST

Figure 15a.

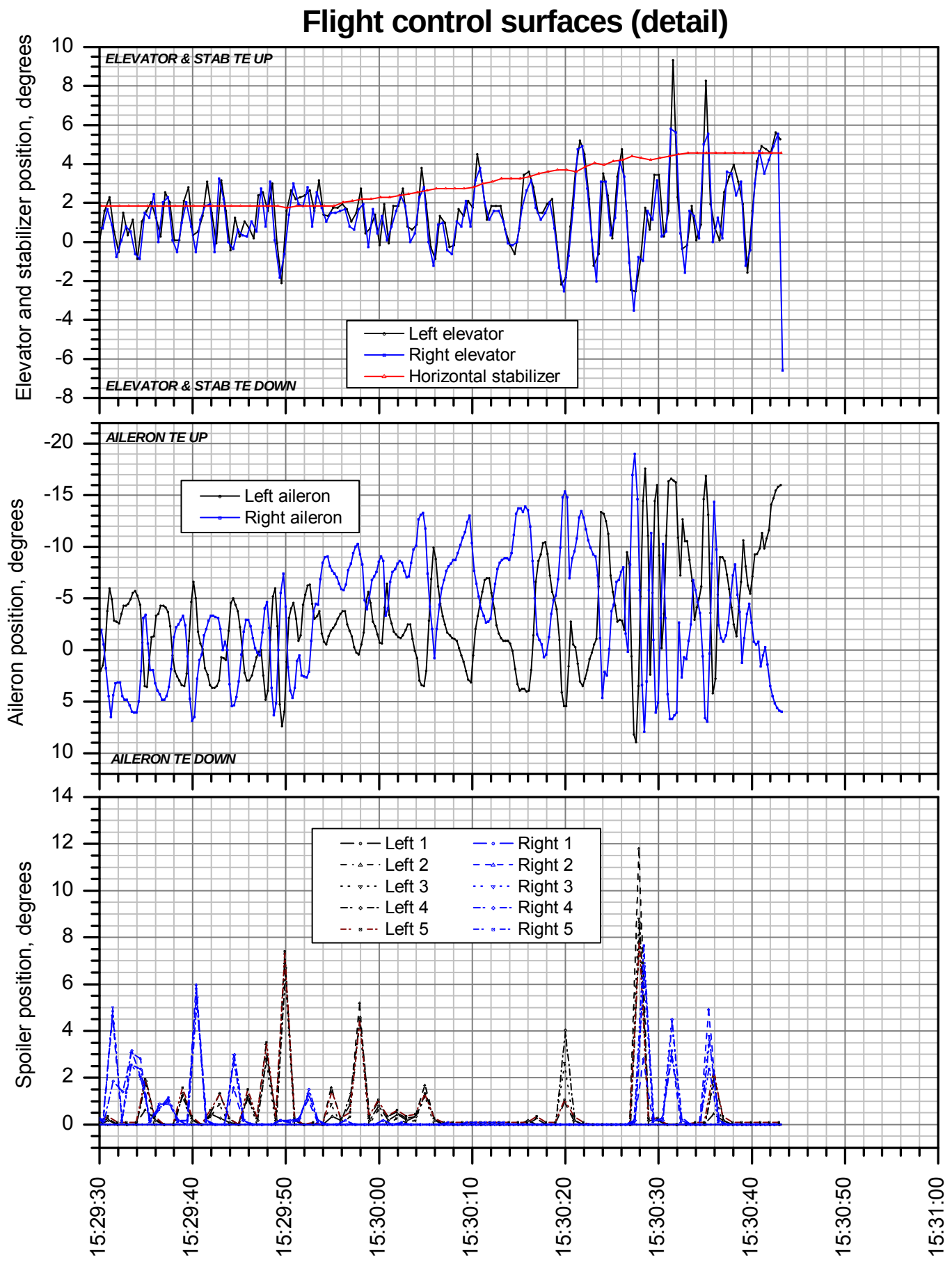
Flight control surfaces (detail)
Elevator and stabilizer position, degrees
ELEVATOR & STAB TE UP
ELEVATOR & STAB TE DOWN
Left elevator
Right elevator
Horizontal stabilizer
Aileron position, degrees
AILERON TE UP
AILERON TE DOWN
Left aileron
Right aileron
Spoiler position, degrees
Left 1
Left 2
Left 3
Left 4
Left 5
Right 1
Right 2
Right 3
Right 4
Right 5
15:29:30
15:29:40
15:29:50
15:30:00
15:30:10
15:30:20
15:30:30
15:30:40
15:30:50
15:31:00
EWR ASR time, HH:MM:SS EST

Figure 15b.

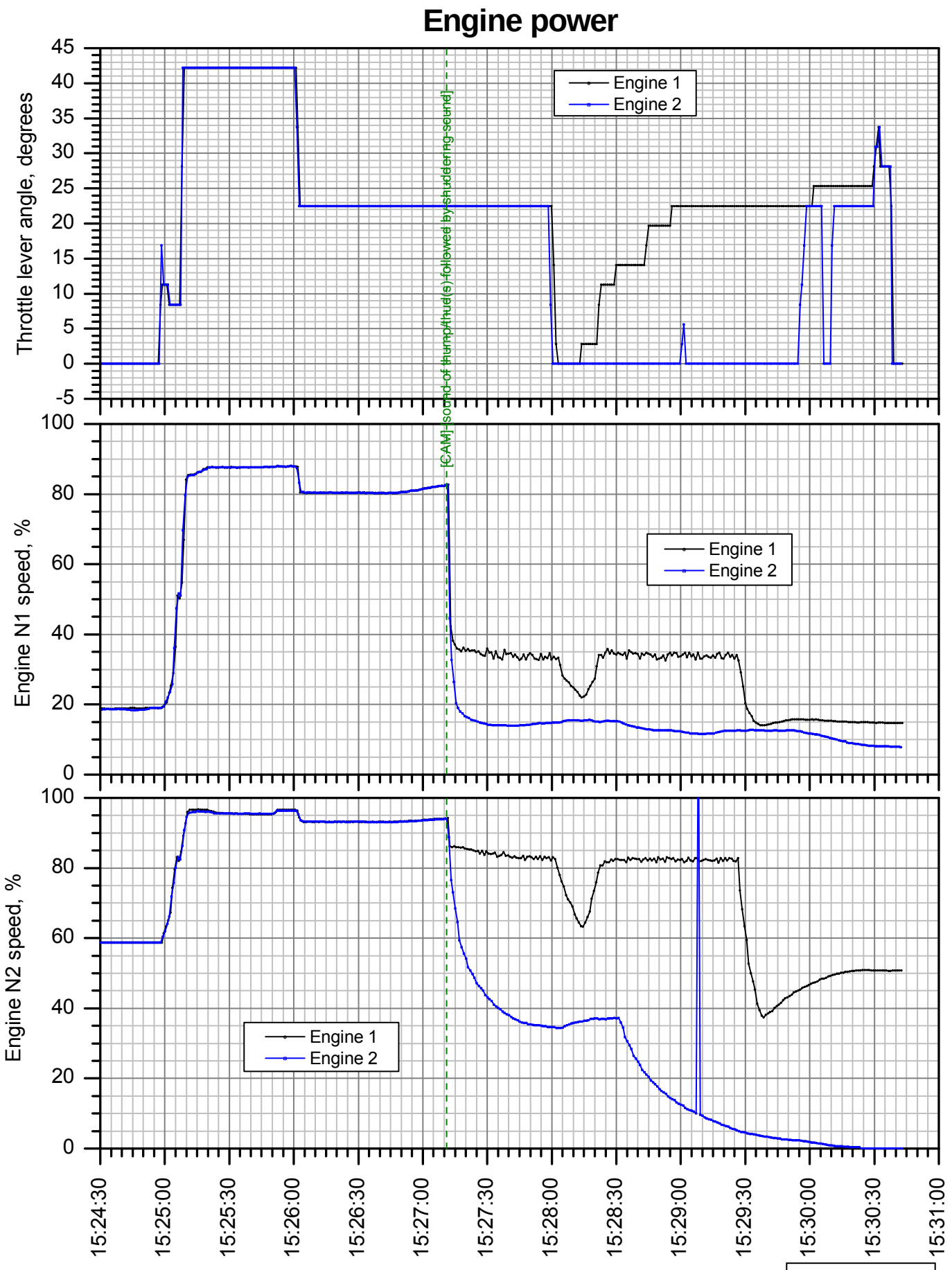
Engine power
Throttle lever angle, degrees
Engine N1 speed, %
Engine N2 speed, %
Engine 1
Engine 2
[CAM] sound of thump/thud(s) followed by shuddering sound
15:24:30
15:25:00
15:25:30
15:26:00
15:26:30
15:27:00
15:27:30
15:28:00
15:28:30
15:29:00
15:29:30
15:30:00
15:30:30
15:31:00
EWR ASR time, HH:MM:SS EST

Figure 16a.

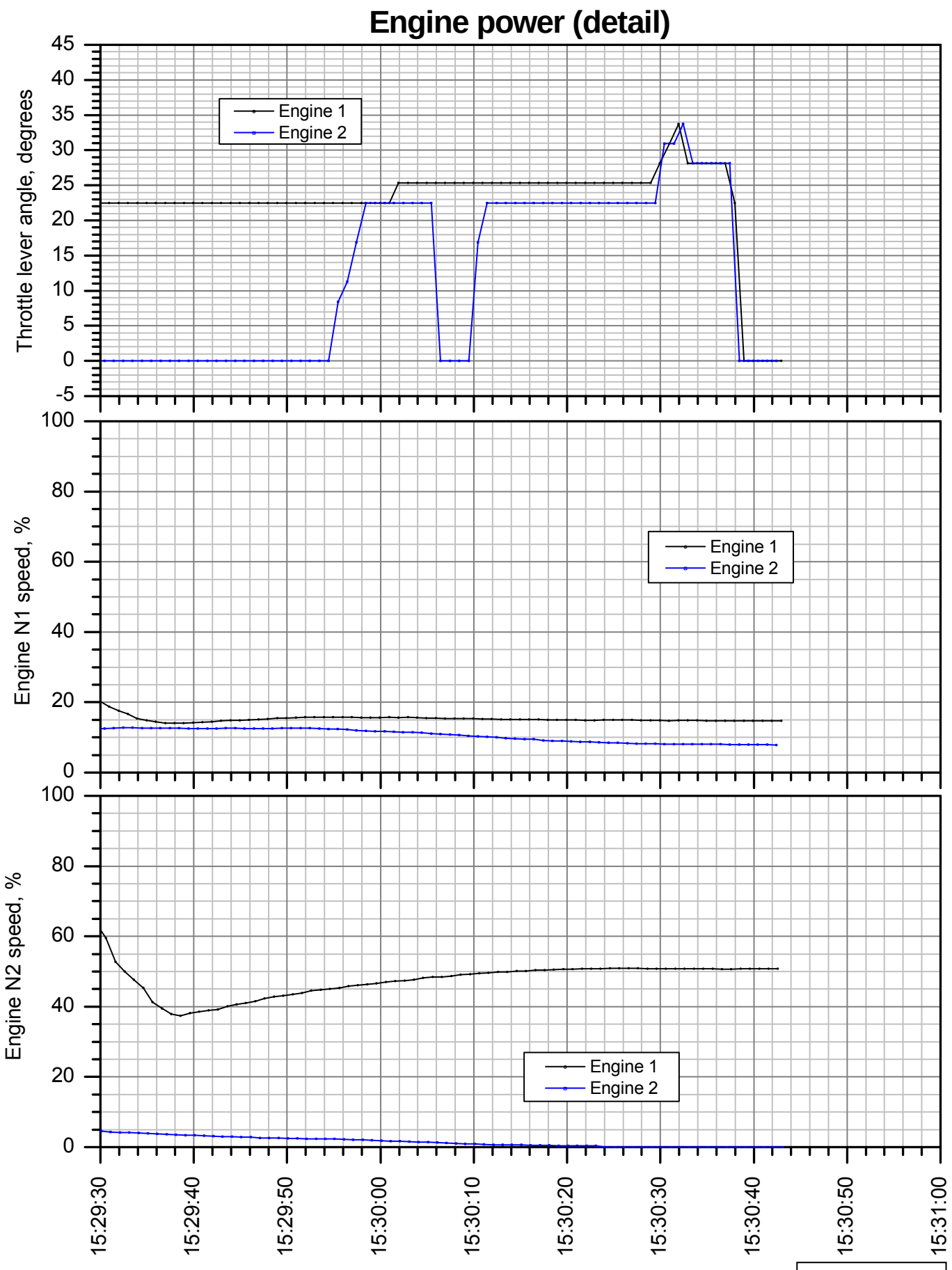
Engine power (detail)
Throttle lever angle, degrees
45
40
35
30
25
20
15
10
5
0
-5
Engine 1
Engine 2
Engine N1 speed, %
100
80
60
40
20
0
Engine 1
Engine 2
Engine N2 speed, %
100
80
60
40
20
0
Engine 1
Engine 2
15:29:30
15:29:40
15:29:50
15:30:00
15:30:10
15:30:20
15:30:30
15:30:40
15:30:50
15:31:00
EWR ASR time, HH:MM:SS EST

Figure 16b.

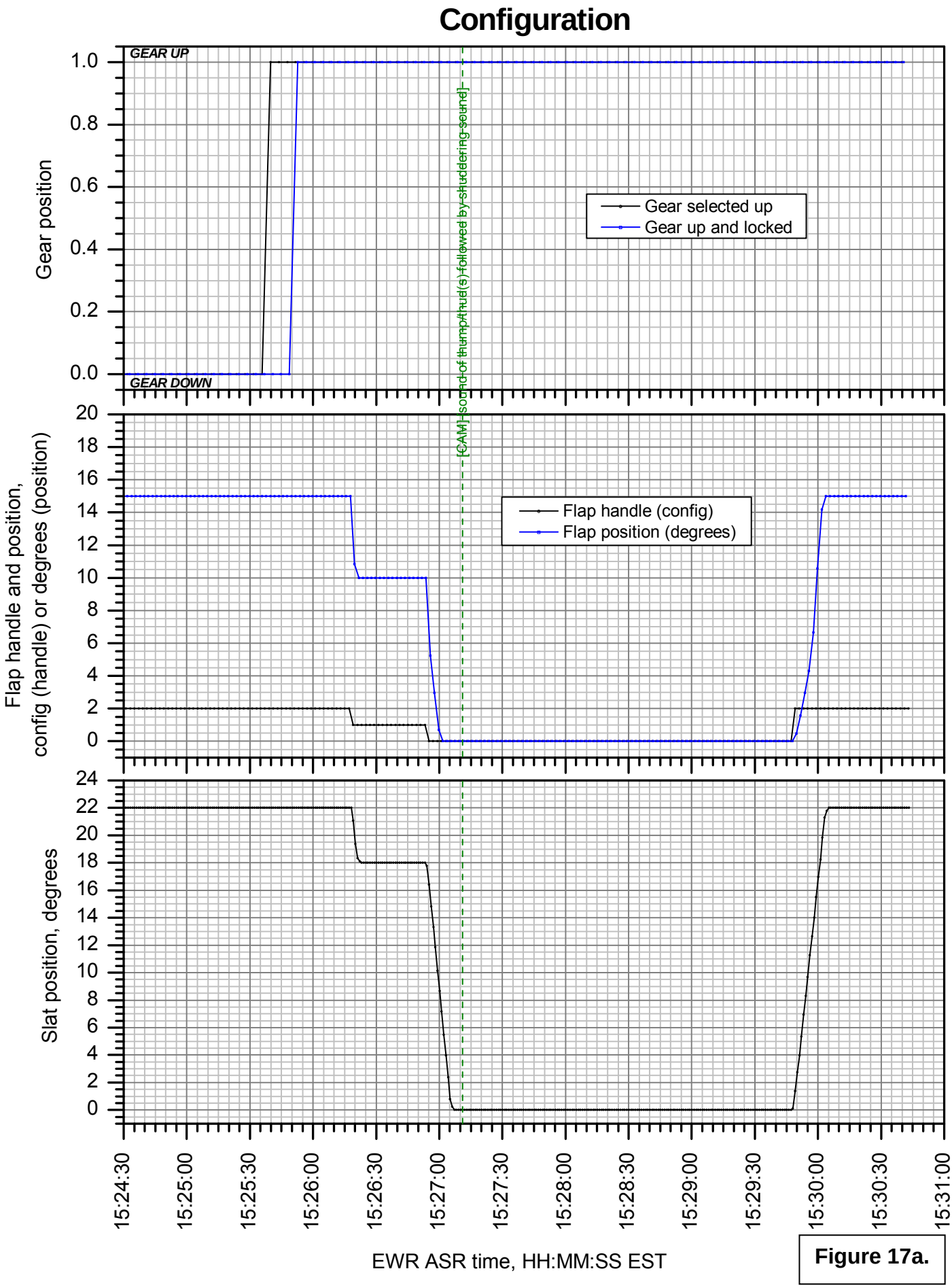
Configuration
GEAR UP
GEAR DOWN
Gear position
Gear selected up
Gear up and locked
[CAM] sound of thump/thud(s) followed by shuddering sound
Flap handle and position, config (handle) or degrees (position)
Flap handle (config)
Flap position (degrees)
Slat position, degrees
15:24:30
15:25:00
15:25:30
15:26:00
15:26:30
15:27:00
15:27:30
15:28:00
15:28:30
15:29:00
15:29:30
15:30:00
15:30:30
15:31:00
EWR ASR time, HH:MM:SS EST

Figure 17a.

Configuration (detail)

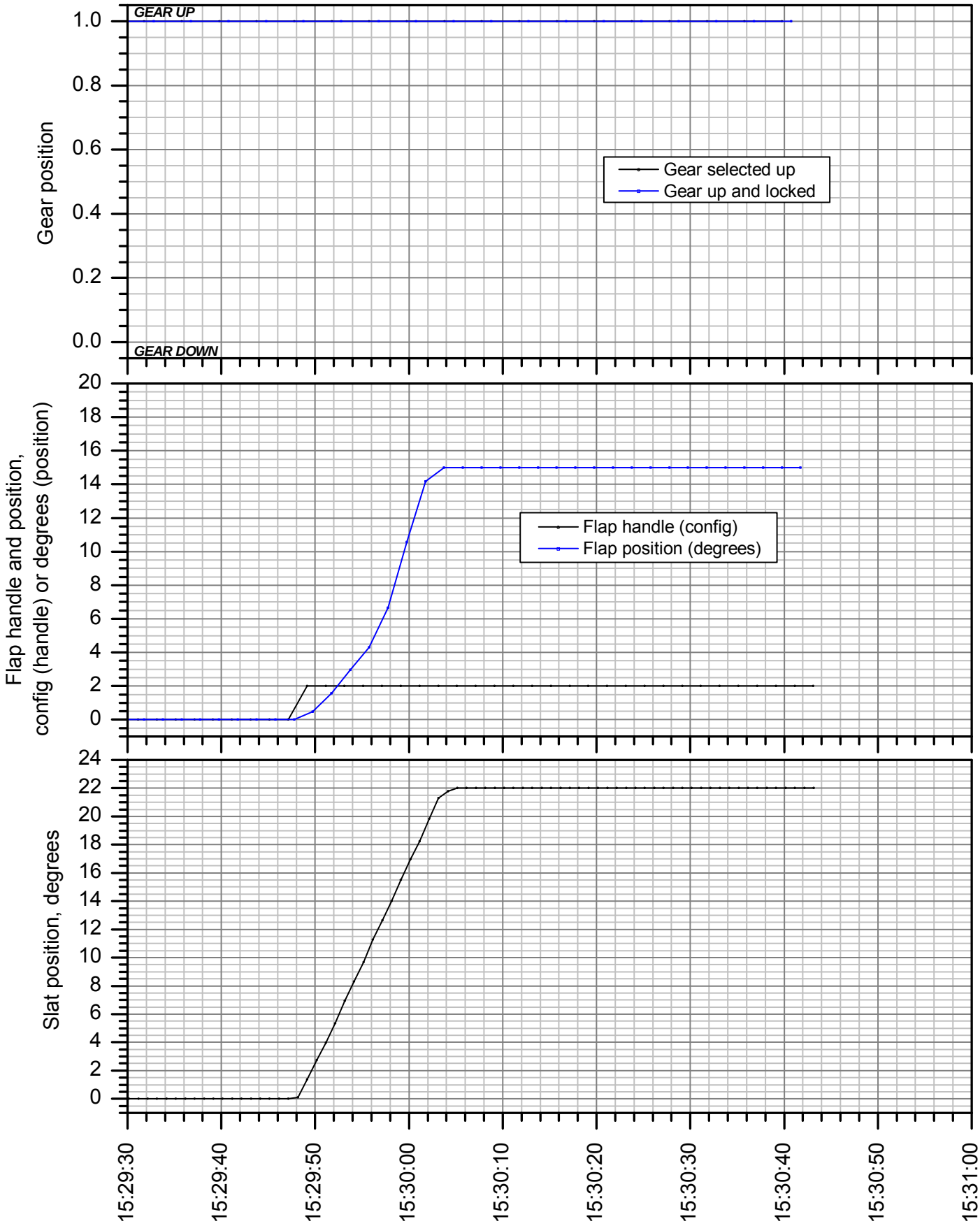

Figure 17b.

THIS PAGE INTENTIONALLY BLANK